

# Exact Formulation of the Resonant Coupling of a Deep-Subwavelength Particle in a Rectangular Conducting Cavity: Beyond the Jaynes-Cummings Model

Koffi-Emmanuel Sadzi<sup>1,\*</sup> and Yakir Hadad<sup>1,†</sup>

<sup>1</sup>*School of Electrical Engineering, Tel Aviv University, Israel, 69978<sup>‡</sup>*

We investigate the resonant interaction between a deep-subwavelength particle and a perfectly conducting rectangular cavity, with potential applications in cavity classical and quantum electrodynamics and wave physics. The particle may behave as a harmonic oscillator, such as a semiconductor plasmonic nanoparticle, a ferrite particle, or as a two-level system, such as a Rydberg atom or trapped ion operating in the microwave regime, where metals can modeled as perfect conductors at microwave frequencies. Our primary objective is to determine the joint resonances (eigenfrequencies) of the coupled cavity-particle system without imposing restrictions on the coupling strength. Unlike conventional quantum optics models, such as the Jaynes-Cummings model, which typically considers interactions with a limited number of cavity modes and may suffer from causality violations, our formulation fully accounts for the complete mode spectrum of the cavity, ensuring strict causality. From a mathematical standpoint, we introduce a novel singularity extraction technique (renormalization) for the local field Green's function,  $G^{\text{loc}}(r)$ , which represents the field at the particle's location due to backscattering of its own radiation. This function is defined as the difference between the cavity Green's function and its free-space counterpart, resulting in a numerically challenging  $\infty - \infty$  form. To precisely calculate this limit, we develop a stable and efficient recursive approach tailored for a rectangular cavity, which can be easily applied to other structured cavities and waveguides. Once  $G^{\text{loc}}(r)$  is determined, we derive the effective polarizability dyadic of the particle within the cavity, given by  $\alpha_{\text{eff}} = [\alpha^{-1} - G^{\text{loc}}(r)]^{-1}$  where  $\alpha$  denotes the particle's dynamic polarizability in free space. The collaborative resonance frequencies of the coupled system,  $\omega_r$ , are then obtained by solving  $\det[\alpha_{\text{eff}}^{-1}(\omega_r)] = 0$ . This formulation enables numerically stable and computationally efficient determination of the system's eigenfrequencies, as demonstrated in several examples with isotropic, gyrotropic, and chiral particles.

## I. INTRODUCTION

The interaction between light and matter is central to numerous scientific and technological advancements. A key strategy for controlling this interaction is to manipulate the photonic environment in which the matter is embedded. A well-established approach is to place the matter inside resonant cavities [1, 2] or optical microcavities [3–7]. Perhaps the most well-known manifestation of this effect is the Purcell effect, where spontaneous emission rates can be enhanced or inhibited by tailoring the emitter's environment, such as resonating [8–15] or reflecting [16, 17] structures. Beyond modifying emission properties, cavity quantum electrodynamics enables applications in molecular dynamics control [5, 18–23] and quantum sensing and computing [24–27]. In such systems, the resonating particles not only interact with an externally applied electromagnetic field but also respond to fields scattered by the cavity boundaries.

In the strong-coupling regime, where the particle's resonant lifetime  $\tau_p$  exceeds the typical wave bouncing time inside the cavity  $\tau_B \sim d/c$  (where  $d$  is the characteristic cavity dimension and  $c$  is the speed of light in vacuum),

the backscattered field from the cavity walls significantly alters the excitation of the particle. Traditionally, this interaction is modeled using a few cavity modes within the framework of the Jaynes-Cummings (JC) model [28, 29]. The rotating wave approximation is often employed for relatively weak coupling, providing reasonable agreement with experimental setups [19, 20]. However, these approaches impose inherent limitations, such as violations of causality [29, 30], and are inadequate for describing arbitrarily strong coupling scenarios.

The subtraction process also termed renormalization of the cavity Green's function in the context of cavity quantum electrodynamics, leads to important consequences. For example, the imaginary and real parts of the renormalized Green's function are directly associated with the spontaneous decay rate and the Lamb shift of the emitter in the cavity. Despite its importance, renormalization is typically done heuristically using, for example, an artificial cutoff for the modes in the cavity or calculating the Green's function at some finite small distance away from the source rather than precisely on the source. In this work, we suggest an *exact and stable* renormalization formalism and an efficient calculation methodology for the mutual coupling process for arbitrary coupling wherein the particle is modeled by a polarizability function  $\underline{\alpha}(\omega)$ . Within classical and semi-classical models, this function encapsulates the material and geometric properties of the particle, linking the induced dipole moment to the so-called *local field*—the field at the particle's position in the absence of the particle itself. In the presence of cav-

\* sadzi@mail.tau.ac.il

† hadady@eng.tau.ac.il

‡ Copyright 2024 by the authors. This article is distributed under a Creative Commons Attribution 4.0 (CC BY) License; This material has been submitted to Physical Review Applied.

ity boundaries, the local field consists of contributions from backscattered waves by the cavity walls.

To rigorously determine the local field it is essential to express the dyadic Green's function within the structured bounded medium in a form that permits its *decomposition* into *primary* and *secondary* components, where the primary is the free space Green's function. While this decomposition may always be *formally* possible. Practically, it may be formidable from a numerical standpoint. This challenge arises because, although the singularity structure near a dipole source remains the same with and without boundaries, the mathematical representations of the Green's function differ significantly, making direct subtraction numerically unstable.

In this paper, we develop an exact, efficient, and numerically robust *ladder-type recursive subtraction approach* to derive the local Green's function in a rectangular cavity. Our methodology leverages alternative representations of the Green's function, facilitating its decomposition in properly selected geometries.

The proposed formulation applies to general dyadic Green's functions, making it suitable for electric, magnetic, and chiral particles. Additionally, our approach can be readily applied for regularization in waveguides, and be extended to other cavity and waveguide geometries that are separable in cylindrical or spherical coordinates. Using this framework, we analyze several cavity-particle systems exhibiting strong coupling with multiple cavity modes, including isotropic particles, anisotropic gyroscopic particles, and biisotropic chiral particles.

The paper is organized as follows: In Sec. II, we introduce the recursive ladder subtraction approach. Section III derives the alternative representations of the Green's functions for rectangular cavities, waveguides, and free space, specifically for an electric dipole along the  $z$ -axis. Appendix C extends the analysis to the magnetic dipole case. Section IV generalizes the derivation to arbitrarily oriented dipole sources. Finally, in Sec. V, we apply the derived local Green's function to calculate the eigenfrequencies of various particle-cavity systems involving isotropic, gyroscopic, and chiral resonant particles.

## II. MATHEMATICAL METHODOLOGY

### A. The Discrete Dipole Approximation

The problem setup is illustrated in Fig. 1. It consists of a deep-subwavelength resonant particle enclosed within a metallic cavity. Our objective is to determine the resonance frequencies (eigenfrequencies) of the coupled system for an arbitrary coupling strength, including cases where the particle exhibits bi-anisotropic properties.

Given the inherent characteristics of the problem—specifically, the significant disparity between the particle and cavity dimensions—the most suitable approach is a volume integral equation formulation [31, 32]. Furthermore, since the particle is assumed to be deep-

subwavelength, a valid approximation in various meta-material and quantum optics scenarios [32, 33], its response can be effectively described by a dipole moment while neglecting higher-order multipoles [34, 35].

Consequently, the integral equation formulation simplifies to the discrete dipole approximation (DDA), a well-established technique used to analyze the microscopic behavior and collective excitation of small particle ensembles at subwavelength scales [32, 33].

Within this framework, the induced dipolar excitation on the particle  $\mathbf{s} = [\mathbf{p}; \mathbf{m}]$  consists of electric and magnetic dipole moments and is related to the local field,  $\mathbf{U}_{\text{loc}} = [\mathbf{E}_{\text{loc}}; \mathbf{H}_{\text{loc}}]$ , i.e., the field at the particle location but in the absence of the particle itself, via,

$$\mathbf{s} = \underline{\underline{\alpha}} \mathbf{U}_{\text{loc}}. \quad (1)$$

where the polarizability tensor,  $\underline{\underline{\alpha}}$ , characterizes the particle and encapsulates both its material properties and geometry. In  $\mathbf{s}$ , and  $\mathbf{U}_{\text{loc}}$ , the semicolon denotes vertical concatenation, and  $\mathbf{p}$ ,  $\mathbf{m}$ ,  $\mathbf{E}_{\text{loc}}$ , and  $\mathbf{H}_{\text{loc}}$  are column vectors representing the electric and magnetic dipole moments, and the electric and magnetic local fields, respectively. In the general case, the polarizability matrix is a  $6 \times 6$  tensor, accounting for both electric and magnetic interactions. Since the particle is assumed to be deep subwavelength, its excitation can be approximated conveniently by a quasi-static solution of Maxwell's equations with uniform field excitation. This calculation leads to the so-called *static polarizability*, denoted by  $\underline{\underline{\alpha}}_s$ , and can be expressed in general as

$$\underline{\underline{\alpha}}_s = \begin{bmatrix} \underline{\underline{\alpha}}_{ee} & \underline{\underline{\alpha}}_{em} \\ \underline{\underline{\alpha}}_{me} & \underline{\underline{\alpha}}_{mm} \end{bmatrix} \quad (2)$$

where  $\underline{\underline{\alpha}}_{ee}$  and  $\underline{\underline{\alpha}}_{mm}$  correspond to electric (magnetic) dipole excitation due to electric (magnetic) local field, whereas  $\underline{\underline{\alpha}}_{em}$  and  $\underline{\underline{\alpha}}_{me}$  account for electric-magnetic coupling, such as in chiral or the general bi-anisotropic cases.

To adequately account for the dynamics of the problem, a *radiation correction* term with compliance with energy conservation with radiation to infinity should be added to the quasi-static solution. For a particle located in a homogeneous medium with permittivity and permeability  $\epsilon_0, \mu_0$ , this correction takes a simple and convenient universal form [33],

$$\underline{\underline{\alpha}}^{-1} = \underline{\underline{\alpha}}_s^{-1} + \begin{bmatrix} j \frac{k^3}{6\pi\epsilon_0} \underline{\underline{I}} & \underline{\underline{0}} \\ \underline{\underline{0}} & j \frac{k^3}{6\pi\mu_0} \underline{\underline{I}} \end{bmatrix} \quad (3)$$

where  $\underline{\underline{I}}$  denotes the  $3 \times 3$  unit dyad. In the following, we will provide examples involving purely electric and chiral, i.e., electric-magnetic polarizabilities.

## B. The local field, effective polarizability, and the eigenvalue problem

### 1. Local field

The Green's function in any structured media can be decomposed into a singular term and a non-singular term. For example, when the medium in the *near vicinity* of the source is homogeneous, a physically natural decomposition would be to the free-space Green's function and to a secondary part of the Green's function that accounts for the back-scattering due to the medium structure. In the cavity we have,

$$\underline{\underline{G}}_{\text{CV}}(\mathbf{r}, \mathbf{r}') = \underline{\underline{G}}_{\text{FS}}(\mathbf{r}, \mathbf{r}') + \underline{\underline{G}}^s(\mathbf{r}, \mathbf{r}') \quad (4)$$

where  $\mathbf{r}$  and  $\mathbf{r}'$  denote the observer and source coordinates, respectively. Unless specifically mentioned otherwise, the Green's functions  $\underline{\underline{G}}$  considered here are defined such that

$$\mathbf{U} = j\omega \underline{\underline{G}}\mathbf{s} \quad (5)$$

namely provides the electric and magnetic fields due to electric and magnetic dipole sources. Thus, it can be in general expressed as a  $6 \times 6$  dyand,

$$\underline{\underline{G}} = \begin{bmatrix} \underline{\underline{G}}^{ee} & \underline{\underline{G}}^{eh} \\ \underline{\underline{G}}^{he} & \underline{\underline{G}}^{hh} \end{bmatrix} \quad (6)$$

where superscripts  $ee$  and  $hh$  denote the electric [magnetic] source to electric [magnetic] field parts of the Green's function, while  $eh$  and  $he$  denote the electric [magnetic] source to magnetic [electric] field parts. Since the free-space Green's function  $\underline{\underline{G}}_{\text{FS}}(\mathbf{r}, \mathbf{r}')$  accounts for the source term, the secondary Green's function  $\underline{\underline{G}}^s(\mathbf{r}, \mathbf{r}')$  is a solution to a *homogeneous* (i.e. source-free) Helmholtz equation and therefore it is *regular* in the entire solution domain.

Consider a general bi-anisotropic particle located at  $\mathbf{r}'$  inside a cavity. In this case, the induced electric and magnetic dipole sources on the particle are given by Eq. (1), where  $\mathbf{U}_{\text{loc}}(\mathbf{r}')$  is the local field acting on the particle. Assume that in the absence of the particle, the field in the cavity is given by  $\mathbf{U}_{\text{in}}(\mathbf{r})$ . Then, when placing the particle in the cavity, the local field acting on the particle consists of the *initial* field  $\mathbf{U}_{\text{in}}(\mathbf{r}')$  plus the *back-scattering* radiation of the particle radiation by the cavity walls. Mathematically we can write,

$$\mathbf{U}_{\text{loc}}(\mathbf{r}') \triangleq j\omega \underline{\underline{G}}_{\text{loc}}(\mathbf{r}')\mathbf{s} + \mathbf{U}_{\text{in}}(\mathbf{r}') \quad (7)$$

where  $\mathbf{s}$  denotes the (electric and magnetic) dipolar excitation induced on the particle. Here, we defined the *local field Green's function* as

$$\underline{\underline{G}}_{\text{loc}}(\mathbf{r}') = \underline{\underline{G}}^s(\mathbf{r}', \mathbf{r}'). \quad (8)$$

By definition, the local Green function is regular. In the context of quantum optics, it is often termed the *regularized* Green's function, and it plays an important role in

determining the frequency detuning (also termed Lamb shift) and the broadening (decay rate) of the quantum emitter resonance due to the coupling to the environment in which it is located.

### 2. Effective polarizability

Our goal here is to solve for the induced source excitation  $\mathbf{s}$  on the particle, when located inside the cavity. By using Eq. (7) in Eq. (1) and solving for  $\mathbf{s}$  we get,

$$\mathbf{s} = \left[ \underline{\underline{\alpha}}^{-1} - j\omega \underline{\underline{G}}_{\text{loc}}(\mathbf{r}') \right]^{-1} \mathbf{U}_{\text{in}}(\mathbf{r}') \triangleq \underline{\underline{\alpha}}_{\text{eff}} \mathbf{U}_{\text{in}}(\mathbf{r}'). \quad (9)$$

Here, we defined the effective polarizability  $\underline{\underline{\alpha}}_{\text{eff}}$  as in [32]. Note that in free space,  $\underline{\underline{G}}_{\text{loc}}$  vanishes and thus the effective polarizability coincides with the regular polarizability. However, in the structured medium, the local Green's function adds to the particle's response, both in frequency detuning and broadening of resonances as discussed above.

### 3. The eigenvalue problem

When we look for the eigen-solutions of the coupled system in a closed cavity, the initial field should be set to zero  $\mathbf{U}_{\text{in}}(\mathbf{r}) = 0$ . Then, the resonance frequencies of the coupled particle-cavity system are obtained by enforcing nontrivial solutions to Eq. (9). Namely,

$$\det \left\{ \underline{\underline{\alpha}}_{\text{eff}}^{-1}(\omega) \right\} = 0. \quad (10)$$

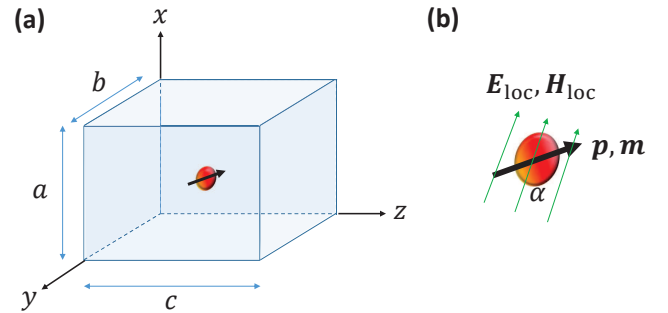


FIG. 1. The physical setup considered in this work. (a) A resonant particle is located inside a conducting rectangular cavity with dimensions  $a, b, c$  along the  $x, y, z$  coordinates. The particle is located at  $\mathbf{r}' = (x', y', z')$  and, in general, can be bi-anisotropic, responding to electric and magnetic fields. The particle, shown in (b) is excited by a local field  $\mathbf{U}_{\text{loc}} = [\mathbf{E}_{\text{loc}}; \mathbf{H}_{\text{loc}}]$ . The excitation is assumed dipolar, where the induced dipoles, electric and magnetic,  $\mathbf{s} = [\mathbf{p}; \mathbf{m}]$  are related to the local fields via the polarizability tensor  $\underline{\underline{\alpha}}$ .

### C. The numerical challenge in calculating $\underline{\underline{G}}_{\text{loc}}$ and the ladder subtraction approach

Calculating the secondary Green's function at the location of the dipole source, as required for the local field Green's function in Eq. (8) is challenging. Mathematically, we need to subtract the free-space Green's function from the cavity Green's function at the source location. While formally this subtraction should be finite, practically, it is numerically challenging to perform. The reason is that the Green's function in the cavity is expressed as a double summation over a discrete set of modes, while the free space Green's function, is expressed as an integral over a continuum of plane-waves [32, 36]. Thus, mathematically speaking, while the Green's functions in the two media do necessarily have the same three-dimensional singularity at the source point [37], their direct subtraction in the physical domain is impossible numerically since it involves an  $\infty - \infty$  structure.

#### 1. Possible remedies

A tempting approach is to use the well-known method of images. However, this becomes cumbersome and computationally expensive because the method of images yields a 3D array of particles. Also, this approach may impose additional challenges when the particle is not located at the center of the cavity. Alternatively, image theory can be used to derive the collective polarizability of a dipole particle in a rectangular waveguide. This will be calculated by 2D summation of the fields from image dipoles, reflected by the walls. As a result, one has a direct relation between the incident field (waveguide mode) and the excited moment. The imaginary part of the collective polarizability may be obtained in a closed form, where we anticipate phenomenologically that the  $k^3/6\pi\epsilon_0$  term (radiation into the free space) is canceled, and instead, a new term corresponding to radiation in a waveguide appears. Variations of these 2D summations for quasistatic fields can be found in [36]. Then, since we also have standard formulas for the amplitudes of the waveguide modes excited by a dipole, one may, in principle, solve for the cavity resonator by considering this dipole in the field of the counter-propagating modes in the waveguide. However, this approach will be cavity mode dependent on deriving the proper radiation correction, and the summation over the 2-dimensional images may be slowly converging if the cavity dimensions along the plane on which the images are calculated are not small on the wavelength.

The Ewald summation technique [38–41] is another possible venue to expedite the summation that results from the use of a brute-force image theory. In our context, it has been used to significantly accelerate the calculation of the Green's function in a rectangular cavity [42]. However, this approach may be more challenging if we are interested in an operation regime that involves

higher-order cavity modes since, in this case, the cavity becomes larger on the wavelength, and the decomposition into the space domain and spatial domain summation may be problem-dependent. Additional challenges arise when the particle is not located in the center of the cavity, where the series of images results in a fundamental lattice with additional sublattices. This issue, however, is incorporated in detail in [41]. In addition, the singularity subtraction issue is still present, and an analytical approach akin to that is used in [33, 43–45] may be applied to accommodate a remedy.

On the other hand, analytical approximated approaches, like perturbation theory, would fall short in the strong coupling regime, which is of interest in many realistic scenarios. Particularly when coupling between the particle to several cavity modes or the coupling between different cavity modes by the particle is of interest.

#### 2. The ladder subtraction approach

Here we suggest an exact and numerically stable and computationally efficient approach for the calculation of the local field Green's function that is applicable for any cavity dimensions, for arbitrary coupling strength, and for different types of coupling mechanism, electric, magnetic, and bi-anisotropic. Thus, providing a practical solution for complex scenarios. The approach relies on using alternative representations of the Green's functions in bounded domains, using a ladder-type subtraction approach, as discussed in the following.

Our goal is to calculate the secondary Green's function at the source location. Following Eq. (4), we need to subtract the free space Green's function from the cavity Green's function. However, as discussed above, directly performing this subtraction will yield an unstable numerical result. To overcome this challenge, we suggest adding and subtracting Green's function in rectangular waveguide  $\underline{\underline{G}}_{\text{RG}}$  and in parallel plate waveguide  $\underline{\underline{G}}_{\text{PP}}$  in the way shown below,

$$\mathbf{G}^s(\mathbf{r}') = \underline{\underline{G}}_{\text{CV}}(\mathbf{r}', \mathbf{r}') - \underline{\underline{G}}_{\text{FS}}(\mathbf{r}', \mathbf{r}') \quad (11a)$$

$$\begin{aligned} &= \underbrace{\underline{\underline{G}}_{\text{CV}}(\mathbf{r}', \mathbf{r}') - \underline{\underline{G}}_{\text{RG}}(\mathbf{r}', \mathbf{r}')}_{\text{Sub. (I)}} \\ &+ \underbrace{\underline{\underline{G}}_{\text{RG}}(\mathbf{r}', \mathbf{r}') - \underline{\underline{G}}_{\text{PP}}(\mathbf{r}', \mathbf{r}')}_{\text{Sub. (II)}} \\ &+ \underbrace{\underline{\underline{G}}_{\text{PP}}(\mathbf{r}', \mathbf{r}') - \underline{\underline{G}}_{\text{FS}}(\mathbf{r}', \mathbf{r}')}_{\text{Sub. (III)}}. \end{aligned} \quad (11b)$$

Thus, the single numerically unstable subtraction is turned to a sum over three subtractions, 'Sub' I, II, and III. The key idea is that each one of these subtractions can become numerically stable and rapidly converging, if the expansion basis of the two Green's functions in the subtraction is the same. In that case, the subtraction

can be performed inside the Green's function expansion. To achieve that, each one of the waveguide Green's functions will be written in two alternative representations, as required to guarantee identical Green's function basis in each subtraction.

The ladder-type subtraction comprises segmenting the secondary Green's extraction into independent subtractions as shown in Eqs. (11b). In the context of a rectangular cavity, we distinguish three subtractions: *Sub. (I)* is the subtraction between the *dyadic* Green's functions of a rectangular cavity (CV) and the ones of the appropriate infinite rectangular waveguide (RG); the second subtraction *Sub. (II)* is between the *dyadic* Green's functions of the same RG and the ones of the appropriate infinite parallel plate waveguide (PP); and last, *Sub. (III)* is the subtraction between the *dyadic* Green's functions of a previously defined PP waveguide and the ones of free space (FS). However, we make use of different alternative representations of the *dyadic* Green's functions of RG in *Sub. (I)* and *Sub. (II)* and similarly in the case of PP waveguide in *Sub. (II)* and *Sub. (III)*. We could, therefore, choose the alternative representations such that the subtractions always take place between 3D Green's functions that exhibit the same eigenmodes along the "transverse" dimension but differ only by their 1-D "longitudinal" Green's function. Hence, the challenging 3D singularity subtraction reduces to three trivial subtractions of regular 1D Green's functions, accelerating the convergence of each subtraction.

The Green's function formalism (Appendix A), which is based on [46] (Ch. 2 and 3) guides the expressions of the Green's functions in each subtraction. Based on the formalism, the rectangular cavity dyadic Green's functions are readily a double summation over discrete spectrum of eigenvalues with coefficients obtained by a 1D finite TL problem, whereas the free space yields a double integral over a continuum of eigenvalues with coefficients obtained by a 1D infinite TL problem [32, 36, 46]. Those already impose the choice of the alternative representation for RG in *subs. (I)* and *subs. (III)* respectively. The choice of the alternative representations in *subs. (II)* comes also naturally as the only one common to both waveguides, namely with the same eigenvalue spectrum—a set of continuum eigenvalues and a set of discrete eigenvalue in the transverse plane. For a succinct description of the form of a typical subtraction, see (Appendix B).

### III. DETAILED DERIVATION OF THE LOCAL GREEN'S FUNCTION IN RECTANGULAR CAVITY

In this section, we detail the singularity subtraction process that is outlined in Eq. (11b). We provide the complete derivation for an electric dipole source oriented along the  $\hat{z}$  direction, and later, using a change of coordinates we obtain the local electric Green's function dyad for arbitrary electric dipole source. Final expressions are

provided, also for the magnetic Green's function dyad connecting a magnetic dipole source to the local magnetic field, and for the cross Green's functions connecting electric source to the local magnetic field, and vice versa.

#### A. Local electric and magnetic Green's function due to an electric current Source with current distribution $\mathbf{J} = J_0\delta(\mathbf{r} - \mathbf{r}')\hat{z}$ inside the cavity

##### 1. Electric Green's functions in the cavity and in a rectangular waveguide infinite along the $z$ -axis

Here we developed the Green's functions involved in *Sub. (I)*. For a  $\hat{z}$  oriented current source located at  $\mathbf{r} = \mathbf{r}'$  inside the cavity (see Fig. 2(a) for illustration),  $\hat{z}$  is defined as the longitudinal axis and the Green's function formalism (Appendix A) is applied. This choice of longitudinal axis reduces the computational cost as it would result in an E-mode only problem, as explained further below. By duality, one would have H-mode only problem in the case of magnetic source along  $\hat{z}$  (see Appendix (C)).

We first perform an eigenmode decomposition in the  $xy$  plane. The boundaries of the cavity are illustrated in Fig.(2)(a), enforcing the standard conditions on an ideal electric conductor surface. The medium inside the cavity is vacuum. The transverse eigenvectors are given for E-mode and H-mode problems, via certain derivatives (see Eqs. (A4,A5,A7a)) of the scalar potentials  $\Phi_i(\rho)$ ,  $\Psi_i(\rho)$ , respectively. Where the scalar potential for the E-mode (H-mode) problem,  $\Phi_i(\rho)$  ( $\Psi_i(\rho)$ ) is found by solving the 2D Helmholtz problem formulated in Eq. (A2) (Eq. (A3)). For the boundaries in the transverse problem

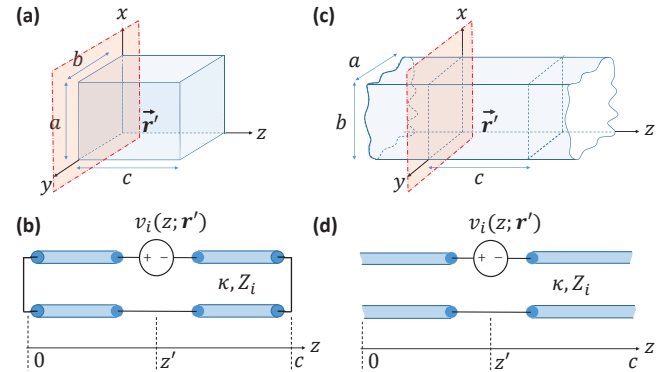


FIG. 2. First subtraction step (*Sub. (I)*). (a) The rectangular cavity with  $\hat{z}$  polarized current dipole source at  $\mathbf{r} = \mathbf{r}'$ . (b) The corresponding longitudinal transmission line problem. (c) An infinite rectangular waveguide with the same dipole source, at the same location as in (a). (d) The longitudinal transmission line model for the waveguide problem. Since the transverse eigenfunctions in the cavity and the waveguide are identical, the singularity subtraction between the problems boils to no more than a simple subtraction of the fields in the 1D TL models (b) and (d).

(on the  $xy$  plane) of the cavity model shown in Fig. 2(a), these potentials read,

$$\Phi_i(\rho) = \frac{2}{\sqrt{ab}} \sin\left(\frac{m\pi x}{a}\right) \sin\left(\frac{n\pi y}{b}\right) \text{ (For E mode)} \quad (12)$$

where  $i = (n, m)$  denoting double indexing, with  $n, m = 1, 2, 3, \dots$ , and

$$\Psi_i(\rho) = \sqrt{\frac{\epsilon_m \epsilon_n}{ab}} \cos\left(\frac{m\pi x}{a}\right) \cos\left(\frac{n\pi y}{b}\right) \text{ (For H mode)} \quad (13)$$

where  $0 \leq n, m \leq \infty$ , and  $\epsilon_m = 2 - \delta[m]$  where  $\delta[m]$  denotes Kronecker's delta function. Once the transverse eigenmodes are known, the fields can be expanded by Eq. (A8a-A8d) for  $M_z = 0$  and  $J_z = \delta(\mathbf{r} - \mathbf{r}')\hat{z}$  (we set  $J_0 = 1[\text{Am}]$ ). The expansion coefficients  $V_i(z)$  and  $I_i(z)$  in Eqs. (A8a-A8d) are obtained by solving the longitudinal problem of the 1D transmission line (TL) along the  $z$ -axis. For the cavity problem, the TLs are shorted for the at  $z = 0, b$ , and characterized by a modal impedance  $Z_i$  and modal longitudinal wavenumber  $\kappa_i$ . A sketch of the model is shown in Fig. 2(b).

The sources in the TL problem are obtained according to Eqs. (A6a) and (A6b). Specifically, for the E-mode,

$$v_i(z; \mathbf{r}') = j \frac{k'_{t,i}}{\omega \varepsilon} \frac{2}{\sqrt{ab}} \sin\left(\frac{m\pi x'}{a}\right) \sin\left(\frac{n\pi y'}{b}\right) \delta(z - z') \quad (14a)$$

$$i_i(z; \mathbf{r}') = 0 \quad (14b)$$

with  $k_{t,i}^2 = \left(\frac{m\pi}{a}\right)^2 + \left(\frac{n\pi}{b}\right)^2$  whereas for H-mode,

$$v_i(z; \mathbf{r}') = 0, \quad i_i(z; \mathbf{r}') = 0 \quad (15)$$

This calculation for the modal sources implies that H-mode waves are not excited in this particular setup, as expected. And, a current source should be absent as in Fig. 2(b) for all modes.

An identical derivation can be followed to calculate Green's function in an infinite rectangular waveguide (see Fig. 2(c)) with an identical  $xy$  cross-section and identical exciting source. The only difference between the two problems is the 1D TL problem that needs to be solved. Specifically, in the cavity case the TL is shorted at its terminations, while in the rectangular waveguide case the TLs are infinite, enabling the waves to propagate outward with no reflections. The solution of these two TL problems can be easily found for the rectangular waveguide (Fig. 2(d)) it is given by,

$$\mathcal{V}_{\text{RG1},i}(z, z') = -\frac{1}{2} \zeta_{z,z'} \cdot e^{-j\kappa_i|z-z'|} \quad (16a)$$

$$\mathcal{I}_{\text{RG1},i}(z, z') = -\frac{1}{2Z'_i} e^{-j\kappa_i|z-z'|} \quad (16b)$$

while for the cavity problem (Fig. 2(b)) reflections should

be included, leading to,

$$\begin{aligned} \mathcal{V}_{\text{CV},i}(z, z') &= \frac{1}{2(e^{-2j\kappa_i c} - 1)} (\zeta_{z,z'} \cdot e^{-j\kappa_i|z-z'|} \\ &+ e^{-j\kappa(z+z')} - e^{-j\kappa(2c-(z+z'))} - \zeta_{z,z'} \cdot e^{-j\kappa(2c-|z-z'|)}) \end{aligned} \quad (17a)$$

$$\begin{aligned} \mathcal{I}_{\text{CV},i}(z, z') &= \frac{1}{2Z'_i(e^{-2j\kappa h} - 1)} (e^{-j\kappa|z-z'|} \\ &+ e^{-j\kappa(z+z')} + e^{-j\kappa(2h-(z+z'))} + e^{-j\kappa(2h-|z-z'|)}) \end{aligned} \quad (17b)$$

where  $\kappa$  and  $Z_i$  are defined as in (A9),(A10) respectively, and  $\zeta_{z,z'} = \text{sign}(z - z')$ . We define unitless amplitudes:

$$\begin{aligned} \bar{\mathcal{V}}_{\text{RG1}}(z, z') &\triangleq 2\mathcal{V}_{\text{RG1}}(z, z') \\ \bar{\mathcal{I}}_{\text{RG1}}(z, z') &\triangleq 2Z_i \mathcal{I}_{\text{RG1}}(z, z') \\ \bar{\mathcal{V}}_{\text{CV}}(y, y') &\triangleq 2\mathcal{V}_{\text{CV}}(y, y') \\ \bar{\mathcal{I}}_{\text{CV}}(y, y') &\triangleq 2Z_i \mathcal{I}_{\text{CV}}(y, y') \end{aligned}$$

The cavity and the rectangular waveguide dyadic Green's functions exhibit the same singularity at the source; not only that but they are also expressed using the same transverse expansion functions. As a result, the subtraction of these two Green's functions boils down to a straightforward subtraction of their corresponding 1D TL voltages and currents. This subtraction removes the source singularity and enables a much faster exponential convergence of the double summations. Thus, using the modal expansion with the modal sources and the TL solutions above, the subtracted cavity and the RG waveguide dyadic Green's functions for z-oriented electric current are expressed by

$$E_{xz}^{(1)}(\mathbf{r}, \mathbf{r}') = \frac{-2j}{\omega \varepsilon ab} \sum_i (\bar{\mathcal{V}}_{\text{CV},i}(z, z') - \bar{\mathcal{V}}_{\text{RG1},i}(z, z')) k_x S_{ix}(x') S_{iy}(y') C_{ox}(x) S_{iy}(y) \quad (18a)$$

$$E_{yz}^{(1)}(\mathbf{r}, \mathbf{r}') = \frac{-2j}{\omega \varepsilon ab} \sum_i (\bar{\mathcal{V}}_{\text{CV},i}(z, z') - \bar{\mathcal{V}}_{\text{RG1},i}(z, z')) k_y S_{ix}(x') S_{iy}(y') S_{ix}(x) C_{oy}(y) \quad (18b)$$

$$E_{zz}^{(1)}(\mathbf{r}, \mathbf{r}') = \frac{2}{\omega \varepsilon ab} \sum_i (\bar{\mathcal{I}}_{\text{CV},i}(z, z') - \bar{\mathcal{I}}_{\text{RG1},i}(z, z')) \frac{(k'_{t,i})^2}{\kappa} S_{ix}(x') S_{iy}(y') S_{ix}(x) S_{iy}(y) \quad (18c)$$

$$H_{xz}^{(1)}(\mathbf{r}, \mathbf{r}') = \frac{2j}{ab} \sum_i (\bar{\mathcal{I}}_{\text{CV},i}(z, z') - \bar{\mathcal{I}}_{\text{RG1},i}(z, z')) \frac{k_y}{\kappa} S_{ix}(x') S_{iy}(y') S_{ix}(x) C_{oy}(y) \quad (18d)$$

$$H_{yz}^{(1)}(\mathbf{r}, \mathbf{r}') = \frac{-2j}{ab} \sum_i (\bar{\mathcal{I}}_{\text{CV},i}(z, z') - \bar{\mathcal{I}}_{\text{RG1},i}(z, z')) \frac{k_x}{\kappa} S_{ix}(x') S_{iy}(y') C_{ox}(x) S_{iy}(y) \quad (18e)$$

$$H_{zz}^{(1)}(\mathbf{r}, \mathbf{r}') = 0 \quad (18f)$$

where,

$$k_x = \frac{m\pi}{a}, k_y = \frac{n\pi}{b}$$

$$Si_x(t) = \sin(k_x t), Co_x(t) = \cos(k_x t)$$

$$Si_y(t) = \sin(k_y t), Co_y(t) = \cos(k_y t)$$

Note that  $k_x$  and  $k_y$  are index-dependent, but for brevity, we omit this notation. Also the notation  $E_{xz}^{(1)}$  denotes the  $x$  component of the subtracted electric field due to a  $z$  oriented unit electric current element, where the superscript (1) indicates that this subtraction corresponds to the *first* line in Eq. (11b), etc.

At this point, we removed the source singularity from the cavity Green's function, but not by subtracting the free space Green's function. Therefore, the subtracted field cannot be regarded as the local field that applies to a particle that is modeled using polarizability with the standard free-space radiation correction.

In terms of Eq. (11b), we are currently done with the first subtraction line. Next, we should add back the rectangular waveguide Green's function, but using an alternative modal representation that will allow us to perform the second subtraction line in Eq. (11b), where our goal is to eventually subtract the free space Green's function. This is done next.

## 2. Alternative representation of the dyadic Green's functions inside an infinite rectangular waveguide and in parallel plate waveguide

Following the discussion above, we focus now on Sub. (II). Namely, in this section, we should restore

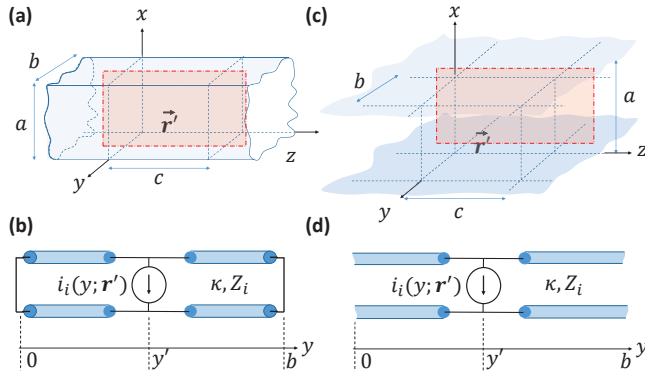


FIG. 3. Second subtraction step (Sub. (II)). (a) The rectangular waveguide with  $\hat{z}$  polarized current dipole source at  $\mathbf{r} = \mathbf{r}'$ . (b) The corresponding longitudinal transmission line problem. As opposed to Fig. 2 here the longitudinal direction is along the  $y$  axis. (c) An infinite parallel plates waveguide with the same dipole source, at the same location as in (a). (d) The longitudinal transmission line model for the parallel plates waveguide problem. Since the transverse eigenfunctions in the rectangular waveguide (in this alternative representation) and the parallel plates waveguide are identical, the singularity subtraction between the problems boils to no more than a simple subtraction of the fields in the 1D TL models (b) and (d).

the field of the rectangular waveguide that we have subtracted before (denoted by RG1). This is achieved using an alternative Green's function representation that is based on a modal expansion on an alternative transverse plane; here it will be the  $xz$  plane instead of the  $xy$  plane i.e.  $y$ -axis is taken as the longitudinal direction. As a result, as opposed to the expansion used in Sec. III A.1 that involved a double sum over two discrete indexes, the present expansion will involve a discrete set of modal functions in  $x$  along which the ideal conductor boundary conditions are enforced at  $x = 0, b$ , and a continuous integration over a parameter  $\xi$  that represents the wavenumber along the  $z$  direction where the waveguide is infinite. With our current choice of the longitudinal axis, it is evident that the problem spans both E- and H-modes as the source is kept in the  $z$ -axis. This choice is also arbitrary as we could easily perform the analysis with a longitudinal  $x$ -axis.

The eigenvector fields resulting from the Helmholtz equations for E-mode Eq. (A2) and H-modes Eq. (A3) are obtained from the scalar potentials  $\Phi_i(\rho)$ ,  $\Psi_i(\rho)$  [46](pp. 252-253) using Eq. (A4,A5,A7a). These potentials are given by,

$$\Phi_i(\rho) = \frac{1}{\sqrt{\pi a}} \sin\left(\frac{m\pi x}{a}\right) e^{-j\xi z} \text{ (For E-modes)} \quad (19a)$$

where  $1 \leq m \leq \infty$ , and

$$\Psi_i(\rho) = \sqrt{\frac{\epsilon_m}{2\pi a}} \cos\left(\frac{m\pi x}{a}\right) e^{-j\xi z} \text{ (For H-modes)} \quad (19b)$$

where  $0 \leq m \leq \infty$ , and  $\epsilon_m = 2 - \delta[m]$ , as before. In both cases,  $-\infty \leq \xi \leq \infty$ .  $i$  denote the index pair  $(\xi, m)$  and  $k_{t,i}^2 = \xi^2 + (m\pi/a)^2$ .

It then remains to solve a 1D transmission line (TL) problem along the  $y$ -axis to obtain the modal voltages and currents  $V_i(y), I_i(y)$  that are required for the field expansion in this case, according to Eqs. (A8a-A8d). To that end, we first need to express the modal sources. Here, the modal voltage source is absent, and both E- and H- modes are present, as opposed to the problem solved in Sec. III A.1. For E-modes, the modal current source reads

$$i_i(y; \mathbf{r}') = -\frac{1}{\sqrt{\pi a}} \frac{j\xi}{k_{t,i}} e^{j\xi z'} \sin\left(\frac{m\pi x'}{a}\right) \delta(y - y') \quad (20a)$$

and for H-modes,

$$i_i(y; \mathbf{r}') = \sqrt{\frac{\epsilon_m}{2\pi a}} \frac{m\pi/a}{k_{t,i}} e^{j\xi z'} \sin\left(\frac{m\pi x'}{a}\right) \delta(y - y') \quad (20b)$$

The rectangular waveguide model is shown in Fig. 3(a), whereas in Fig. 3(b) the corresponding TL model for the RG2 representation is shown. The TL overall length is  $b$  and it is shorted at its terminations, at  $y = 0$  and  $y = b$ . The sources are located at  $y = y'$ . Thus, the TL model for E- and H-modes is the same, except for the specific expression for the characteristic impedance  $Z_i$  that varies between the polarizations and the modes.

The TL problem can be readily solved,

$$\begin{aligned} \mathcal{V}_{\text{RG2},i}(y, y') &= \frac{Z_i}{2(e^{-2j\kappa b} - 1)} (e^{-j\kappa|y-y'|} \\ &- e^{-j\kappa(y+y')} - e^{-j\kappa(2b-(y+y'))} + e^{-j\kappa(2b-|y-y'|)}) \end{aligned} \quad (21\text{a})$$

$$\begin{aligned} \mathcal{I}_{\text{RG2},i}(y, y') &= \frac{1}{2(e^{-2j\kappa b} - 1)} (\varsigma_{y,y'} \cdot e^{-j\kappa|y-y'|} \\ &- e^{-j\kappa(y+y')} + e^{-j\kappa(2b-(y+y'))} - \varsigma_{y,y'} \cdot e^{-j\kappa(2b-|y-y'|)}) \end{aligned} \quad (21\text{b})$$

where  $\kappa$  and  $Z_i$  are defined as in (A9), (A10) respectively, and  $\varsigma_{y,y'} = \text{sign}(y - y')$ .

This modal solution can be used to expand the electric and magnetic fields that are excited in the rectangular waveguide problem. These fields, although expressed differently, are completely equivalent to the rectangular waveguide fields that were calculated in the previous section using the first modal representation denoted by RG1. Thus, when we subtract the fields RG1 and add the fields RG2 to the cavity field we end up with the original (singular) cavity field. However, as we discussed before, the subtraction result of RG1 from the cavity field is completely regular. Therefore, now, to maintain regularity, we should subtract the singular term from RG2. To that end, we use the Green's function in the parallel plate waveguide that is shown in Fig. 3(c). The corresponding TL model for this problem is shown in Fig. 3(d). Since the two models (in Fig. 3(b) and Fig. 3(d)) are identical except for the boundary, it immediately follows that the subtraction of these modal voltages and currents excludes the source singularity, as required. The modal voltage and current for the parallel plates model read,

$$\mathcal{V}_{\text{PP1},i}(y, y') = \frac{-Z_i}{2} e^{-j\kappa|y-y'|} \quad (22\text{a})$$

$$\mathcal{I}_{\text{PP1},i}(y, y') = \frac{-1}{2} \varsigma_{y,y'} \cdot e^{-j\kappa|y-y'|}. \quad (22\text{b})$$

To simplify the following subtracted field expressions we define unitless amplitudes,

$$\bar{\mathcal{V}}_{\text{RG2},i}(y, y') \triangleq 2Z_i \mathcal{V}_{\text{RG2},i}(y, y')$$

$$\bar{\mathcal{I}}_{\text{RG2},i}(y, y') \triangleq 2 \mathcal{I}_{\text{RG2},i}(y, y')$$

$$\bar{\mathcal{V}}_{\text{PP1},i}(y, y') \triangleq 2Z_i \mathcal{V}_{\text{PP1},i}(y, y')$$

$$\bar{\mathcal{I}}_{\text{PP1},i}(y, y') \triangleq 2 \mathcal{I}_{\text{PP1},i}(y, y')$$

and express below the subtraction of RG2 from the parallel plates field, for the z-oriented electric current element,

$$\begin{aligned} E_{xz}^{(2)}(\mathbf{r}, \mathbf{r}') &= \frac{-j}{2\pi a \omega \varepsilon} \sum_{m \neq 0} S i_x(x') C o_x(x) \\ &\cdot \int_{\xi} d\xi \frac{\xi k_x}{\kappa} (\bar{\mathcal{V}}_{\text{RG2},i}(y, y') - \bar{\mathcal{V}}_{\text{PP1},i}(y, y')) e^{-j\xi(z-z')} \end{aligned} \quad (23\text{a})$$

$$\begin{aligned} E_{yz}^{(2)}(\mathbf{r}, \mathbf{r}') &= \frac{-1}{2\pi a \omega \varepsilon} \sum_{m \neq 0} S i_x(x') S i_x(x) \\ &\cdot \int_{\xi} d\xi \xi (\bar{\mathcal{I}}_{\text{RG2},i}(y, y') - \bar{\mathcal{I}}_{\text{PP1},i}(y, y')) e^{-j\xi(z-z')} \end{aligned} \quad (23\text{b})$$

$$\begin{aligned} E_{zz}^{(2)}(\mathbf{r}, \mathbf{r}') &= \frac{1}{2\pi a \omega \varepsilon} \sum_{m \neq 0} S i_x(x') S i_x(x) \\ &\cdot \int_{\xi} d\xi \frac{\kappa^2 + k_x^2}{\kappa} (\bar{\mathcal{V}}_{\text{RG2},i}(y, y') - \bar{\mathcal{V}}_{\text{PP1},i}(y, y')) e^{-j\xi(z-z')} \end{aligned} \quad (23\text{c})$$

$$\begin{aligned} H_{xz}^{(2)}(\mathbf{r}, \mathbf{r}') &= \frac{1}{2\pi a} \sum_{m \neq 0} S i_x(x') S i_x(x) \\ &\cdot \int_{\xi} d\xi (\bar{\mathcal{I}}_{\text{RG2},i}(y, y') - \bar{\mathcal{I}}_{\text{PP1},i}(y, y')) e^{-j\xi(z-z')} \end{aligned} \quad (23\text{d})$$

$$\begin{aligned} H_{yz}^{(2)}(\mathbf{r}, \mathbf{r}') &= \frac{-j}{2\pi a} \sum_{m \neq 0} S i_x(x') C o_x(x) \\ &\cdot \int_{\xi} d\xi \frac{k_x}{\kappa} (\bar{\mathcal{V}}_{\text{RG2},i}(y, y') - \bar{\mathcal{V}}_{\text{PP1},i}(y, y')) e^{-j\xi(z-z')} \end{aligned} \quad (23\text{e})$$

$$H_{zz}^{(2)}(\mathbf{r}, \mathbf{r}') = 0 \quad (23\text{f})$$

The superscript (2) indicates that these subtracted fields correspond to the *second* line in Eq. (11b). Next, we have to compensate for the subtracted parallel plate waveguide field. To that end, we will add it back but this time using an alternative representation that will allow us to conveniently subtract the free space Green's function field, which is our ultimate result. Note that the parallel plate field expansion here was done along the *xz* plane where, on the *x* axis the structure is finite, thus leading to a discrete set of eigenmodes. The decomposition of the alternative representation will be done along the *yz* plane, where the waveguide of parallel plates is infinite.

### 3. Green's function in free space and the alternative representation of the Green's functions in parallel plates waveguide

Here we focus on *Sub. (III)*. We compensate for the subtracted parallel plates waveguide field PP1 by adding an identical field that is alternatively represented. We denote this representation by PP2. By adding this field to the two subtracted fields in the previous sections, we restore exactly the singular cavity field. However, here we can identify the singularity as a consequence of PP2, and

thus, the subtraction of the free space Green's function becomes trivial. This is elaborated below. To decompose the parallel plates field in the PP2 representation, we choose  $x$ -axis as the longitudinal axis and perform the eigenmode decomposition in the  $yz$  plane. Consequently, the transverse eigenmode problem is infinite in two dimensions (see Fig. 4(a)). For a complete picture, one would remain with the  $y$ -axis as the longitudinal axis if the  $x$ -axis was chosen as the longitudinal axis in the *Sub. (II)* case. The problem would, regardless, span both E- and H-modes, as expressed below. The eigenvector fields resulting from the Helmholtz equations for E-mode (A2) and H-modes (A3) are obtained from scalar potentials  $\Phi_i(\rho)$ ,  $\Psi_i(\rho)$  [46] (pg 251,252) using (A4,A5,A7a)

$$\Phi_i(\rho) \equiv \Psi_i(\rho) = \frac{1}{2\pi} e^{-j\eta y} e^{-j\xi z} \quad (24)$$

where  $-\infty \leq \xi, \eta \leq \infty$ , and  $i$  denotes the index pair  $(\eta, \xi)$ . It then remains to solve a 1D TL problem along the  $x$ -axis to obtain the coefficients  $V_i(x)$ ,  $I_i(x)$  for the field expansion according to (A8a-A8d). The TL model is shown in Fig. 4(b). Up to trivial notation changes  $y \mapsto x$  and  $b \mapsto a$ , the TL problem is identical to the one solved previously for RG2 (see Fig. 3 (b) and the solution in Eq. (21a)). Thus,

$$\mathcal{V}_{\text{PP2},i}(x, x') = \mathcal{V}_{\text{RG2},i}(y, y')|_{x \mapsto y, x' \mapsto y', a \mapsto b} \quad (25a)$$

$$\mathcal{I}_{\text{PP2},i}(x, x') = \mathcal{I}_{\text{RG2},i}(y, y')|_{x \mapsto y, x' \mapsto y', a \mapsto b} \quad (25b)$$

Finally, in order to subtract the free-space Green's function (see Fig. 4(c)) from the alternatively represented parallel plates field PP2 we need to solve the infinite TL

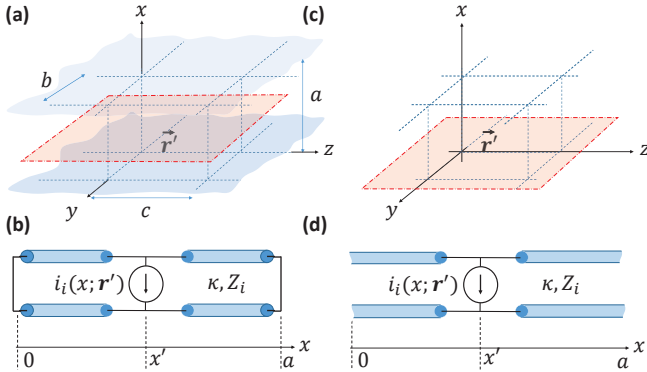


FIG. 4. Third and last subtraction step (*Sub. (III)*). (a) The parallel plates waveguide with  $\hat{z}$  polarized current dipole source at  $\mathbf{r} = \mathbf{r}'$ . (b) The corresponding longitudinal transmission line problem. As opposed to Fig. 3 here the longitudinal direction is along the  $x$  axis. (c) The free space with the same dipole source, at the same location as in (a). (d) The longitudinal transmission line model for the free space problem. Since the transverse eigenfunctions in the parallel plates waveguide (in this alternative representation) and the free space radiation are identical, the singularity subtraction between the problems boils to no more than a simple subtraction of the fields in the 1D TL models (b) and (d).

model that is shown in Fig. 4(d). Again, this problem is nearly identical to the PP1 problem solved for the TL model in Fig. 3(d), and the solution will be immediately found by the same change of variables as done in Eq. (25a). Thus,

$$\mathcal{V}_{\text{FS},i}(x, x') = \mathcal{V}_{\text{PP1},i}(y, y')|_{x \mapsto y, x' \mapsto y', a \mapsto b} \quad (26a)$$

$$\mathcal{I}_{\text{FS},i}(x, x') = \mathcal{I}_{\text{PP1},i}(y, y')|_{x \mapsto y, x' \mapsto y', a \mapsto b} \quad (26b)$$

Next, as previously done, we define unitless amplitudes,

$$\bar{\mathcal{V}}_{\text{PP2},i}(y, y') \triangleq 2Z_i \mathcal{V}_{\text{PP2},i}(y, y')$$

$$\bar{\mathcal{I}}_{\text{PP2},i}(y, y') \triangleq 2\mathcal{I}_{\text{PP2},i}(y, y')$$

$$\bar{\mathcal{V}}_{\text{FS},i}(y, y') \triangleq 2Z_i \mathcal{V}_{\text{FS},i}(y, y')$$

$$\bar{\mathcal{I}}_{\text{FS},i}(y, y') \triangleq 2\mathcal{I}_{\text{FS},i}(y, y')$$

Then, the subtracted field, PP2 minus free-space, reads

$$\begin{aligned} E_{xz}^{(3)}(\mathbf{r}, \mathbf{r}') = & \frac{j}{4\pi\omega\varepsilon} \cos(\bar{\phi}) \\ & \cdot \int_0^\infty dq \frac{q^2}{\kappa} \mathcal{J}_1(q\bar{\rho}) (\bar{\mathcal{I}}_{\text{PP2},i}(x, x') - \bar{\mathcal{I}}_{\text{FS},i}(x, x')) \end{aligned} \quad (27a)$$

$$\begin{aligned} E_{yz}^{(3)}(\mathbf{r}, \mathbf{r}') = & \frac{1}{4\pi\omega\varepsilon} \frac{\sin(2\bar{\phi})}{2} \\ & \cdot \int_0^\infty dq \frac{q^3}{\kappa} \mathcal{J}_2(q\bar{\rho}) (\bar{\mathcal{V}}_{\text{PP2},i}(x, x') - \bar{\mathcal{V}}_{\text{FS},i}(x, x')) \end{aligned} \quad (27b)$$

$$\begin{aligned} E_{zz}^{(3)}(\mathbf{r}, \mathbf{r}') = & \frac{1}{4\pi\omega\varepsilon} \int_0^\infty dq \left[ \frac{q^3}{2\kappa} \cos(2\bar{\phi}) \mathcal{J}_2(q\bar{\rho}) + \right. \\ & \left. q \frac{2k^2 - q^2}{\kappa} \mathcal{J}_0(q\bar{\rho}) \right] (\bar{\mathcal{V}}_{\text{PP2},i}(x, x') - \bar{\mathcal{V}}_{\text{FS},i}(x, x')) \end{aligned} \quad (27c)$$

$$\begin{aligned} H_{xz}^{(3)}(\mathbf{r}, \mathbf{r}') = & \frac{-j}{4\pi} \sin(\bar{\phi}) \\ & \cdot \int_0^\infty dq \frac{q^2}{\kappa} \mathcal{J}_1(q\bar{\rho}) (\bar{\mathcal{V}}_{\text{PP2},i}(x, x') - \bar{\mathcal{V}}_{\text{FS},i}(x, x')) \end{aligned} \quad (27d)$$

$$\begin{aligned} H_{yz}^{(3)}(\mathbf{r}, \mathbf{r}') = & \\ & -\frac{1}{4\pi} \int_0^\infty dq q \mathcal{J}_0(q\bar{\rho}) (\bar{\mathcal{I}}_{\text{PP2},i}(x, x') - \bar{\mathcal{I}}_{\text{FS},i}(x, x')) \end{aligned} \quad (27e)$$

$$H_{zz}^{(3)}(\mathbf{r}, \mathbf{r}') = 0 \quad (27f)$$

Here, superscript (3) indicates that these subtractions correspond to the *third* line in Eq. (11b). Also,  $q^2 = \xi^2 + \eta^2$  and  $(\bar{\rho}, \bar{\phi})$  are the polar coordinate representation of  $(z - z', y - y')$ ;  $\mathcal{J}_n(\cdot)$  denote the  $n$ th order Bessel function of the first kind.

Now, one can write the full expression for the local dyadic Green's function as a sum of three components. For example, for the x-component of the electric field due to a current source in  $\hat{z}$  inside the cavity we have,

$$G_{xz}^{ee}(\mathbf{r}, \mathbf{r}') = \hat{\mathbf{x}}\hat{\mathbf{z}}(E_{xz}^{(1)} + E_{xz}^{(2)} + E_{xz}^{(3)}) \quad (28a)$$

$$G_{xz}^{he}(\mathbf{r}, \mathbf{r}') = \hat{\mathbf{x}}\hat{\mathbf{z}}(H_{xz}^{(1)} + H_{xz}^{(2)} + H_{xz}^{(3)}) \quad (28b)$$

where  $\hat{\mathbf{x}}\hat{\mathbf{z}}$  represents a dyadic product.

#### IV. GENERALIZATION TO THE DYADIC GREEN'S FUNCTIONS FOR GENERAL ELECTRIC AND MAGNETIC CURRENT SOURCE/DENSITY

In Sec. III, we derived local Green's function for an electric source along the  $z$ -axis, and in Appendix C we expand on the magnetic dipole case along  $z$ , all inside a rectangular cavity. Here, we generalize these results for the local dyadic Green's function due to an arbitrarily polarized dipole source.

We can express the electric current source as  $\mathbf{J} = (J_x(\mathbf{r}), J_y(\mathbf{r}), J_z(\mathbf{r}))$  and the magnetic current source as  $\mathbf{M} = (M_x(\mathbf{r}), M_y(\mathbf{r}), M_z(\mathbf{r}))$ . The Green's functions for a electric/magnetic current source in  $\hat{\mathbf{z}}$ , developed in the previous sections, can be used to find the Green's functions for a electric/magnetic current source in the remaining axis, namely  $\hat{x}, \hat{y}$ , in the following steps.

For source in  $\hat{x}$

- We define new coordinate axis  $(x', y', z')$  such that  $x \longleftrightarrow z', y \longleftrightarrow x'$  and  $z \longleftrightarrow y'$  where  $(x, y, z)$  is the original axis
- We define new dimensions  $a', b', c'$  such that  $a \longleftrightarrow c', b \longleftrightarrow a'$  and  $c \longleftrightarrow b'$  where  $(a, b, c)$  are the original dimensions of our original cavity;
- Finally we perform the following substitution:

$$G_{xx}^f \longleftrightarrow G_{z'z'}^f \quad G_{yx}^f \longleftrightarrow G_{x'z'}^f \quad G_{zx}^f \longleftrightarrow G_{y'z'}^f$$

For source in  $\hat{y}$

- We define new coordinate axis  $(x', y', z')$  such that  $x \longleftrightarrow y', y \longleftrightarrow z'$  and  $z \longleftrightarrow x'$  where  $(x, y, z)$  is the original axis
- We define new dimensions  $a', b', c'$  such that  $a \longleftrightarrow b', b \longleftrightarrow c'$  and  $c \longleftrightarrow a'$  where  $(a, b, c)$  are the original dimensions of our original cavity;
- Finally we perform the following substitution:

$$G_{xy}^f \longleftrightarrow G_{y'z'}^f \quad G_{yy}^f \longleftrightarrow G_{z'z'}^f \quad G_{zy}^f \longleftrightarrow G_{x'z'}^f$$

$f$  denote *em,me,ee,or mm* types. We thereby obtained the complete Dyadic Green's function for both electric and magnetic current sources. While we omit for brevity the complete expressions for the electric and magnetic dyadic Green's function. It is fully implemented in our code which will be provided under a reasonable request.

#### V. EXAMPLES

In this section, we use our approach for the local field calculation to study the collective excitation of a resonant plasmonic particle inside a rectangular cavity. For the particle, we assume three cases, first, a spherical particle consists of an isotropic permittivity model, second, a spherical particle consists of a gyrotropic (magnetized) particle and last, a spherical particle with bi-isotropic chiral property. In all cases, we analyze the exact collective excitation without resorting to any approximation regarding the coupling strength or the number of modes that are taken in the coupling process. For our numerical analysis, the dimensions of the rectangular cavity are set as  $a = b = 10\mu\text{m}$ ,  $c = 30\mu\text{m}$ ; The first three cutoff frequencies of the cavity are given by:  $\omega_{1,\text{cv}} \approx 15.81\text{THz}$ ,  $\omega_{2,\text{cv}} \approx 18.03\text{THz}$ , and  $\omega_{3,\text{cv}} \approx 21.21\text{THz}$ . The particle has  $R_o = 1\mu\text{m}$  as radius. Under these conditions, since the particle is small on the wavelength at the cavity's first resonance ( $2R_o \ll 20\mu\text{m}$ ) and on the dimensions of the cavity ( $2R_o \ll a, b, c$ ), we can apply the dipole approximation.

##### A. Analysis of the dynamics of a plasmonic sphere inside the cavity

###### 1. Problem description

As a starting point, we place an isotropic plasmonic sphere in the cavity. Under discrete dipole approximation, the particle is modeled using an electric polarizability. The polarizability tensor of a general ellipsoid of volume  $V$  made of an anisotropic material  $\epsilon$  can be found in [36] for the static case. In the dynamic case, it needs to be augmented to incorporate radiation loss [47]. We model the relative permittivity using the Drude Model with no loss ( $\Gamma = 0$ ), and its relative permeability is set to 1. For the simpler case of a sphere, the dynamic polarizability matrix reduces to,

$$\underline{\underline{\alpha}}^{-1} = \underline{\underline{\alpha}}_e^{-1} = \left( \frac{1}{\varepsilon_0 V} \frac{\varepsilon_r(\omega) + 2}{3(\varepsilon_r(\omega) - 1)} + j \frac{k^3}{6\pi\varepsilon_0} \right) \underline{\underline{I}} \quad (29a)$$

$$\varepsilon_r(\omega) = 1 - \frac{\omega_p^2}{\omega^2} \quad (29b)$$

where  $\omega_p$  denotes that plasma frequency;  $\underline{\underline{I}}$  denote the  $3 \times 3$  identity matrix.

From our above analytical approach, we now have the exact local Green's function for a current source,  $\underline{\underline{G}}^s$ . The expression of the excited dipole moment that is induced on the particle is given by,

$$\mathbf{p} = \underline{\underline{\alpha}}_{\text{eff}} \mathbf{E}_{\text{inc}}(\mathbf{r}', \mathbf{r}') \quad (30)$$

where the effective (also termed - collective) polarizability tensor  $\underline{\underline{\alpha}}_{\text{eff}}$  is expressed as,

$$\underline{\underline{\alpha}}_{\text{eff}}^{-1} = \left[ \underline{\underline{\alpha}}^{-1} - \underline{\underline{\tilde{G}}}^s(\mathbf{r}', \mathbf{r}') \right] \quad (31)$$

and  $\tilde{\underline{\underline{G}}}^s \triangleq j\omega \cdot \underline{\underline{G}}^s$ . The multiplication with  $j\omega$  accounts for the fact that the Green's functions derived in the previous sections are for an infinitesimal current source rather than for a point dipole. This definition is implied and omitted in the rest of the paper.

The static polarizability is corrected to obey energy conservation. Thus, the dynamic polarizability in *free space* reads,

$$\mathcal{I}\{\tilde{\underline{\underline{G}}}^s\} = \mathcal{I}\{\underline{\underline{\alpha}}^{-1}\} = \frac{k^3}{6\pi\varepsilon_0} \underline{\underline{I}}. \quad (32)$$

To study the resonance of the system sphere-cavity, we look for the frequencies that will nullify the determinant of  $\underline{\underline{\alpha}}^{-1}$  in Eq. (31).

## 2. Results and Interpretations

The resonance in the case of the isolated particle is well-known. There are three degenerative eigenmodes at  $\omega = \omega_p/\sqrt{3}$ . In contrast, we analyze the change in the coupled system's resonance frequencies as we vary the particle's plasmonic frequency,  $\omega_p$ . The result is depicted in Fig. 5, where we limit the analysis range for  $\omega_p$  slightly below the 3rd resonance frequency of the empty (isolated) cavity. In this simulation, the cavity dimensions are set such that  $a = b$ , and consequently it supports two degenerative eigenmodes at each resonance frequency inside the empty cavity.

As shown in Fig. 5, the coupling between the cavity and isotropic sphere lifts the degeneracy in the resonant

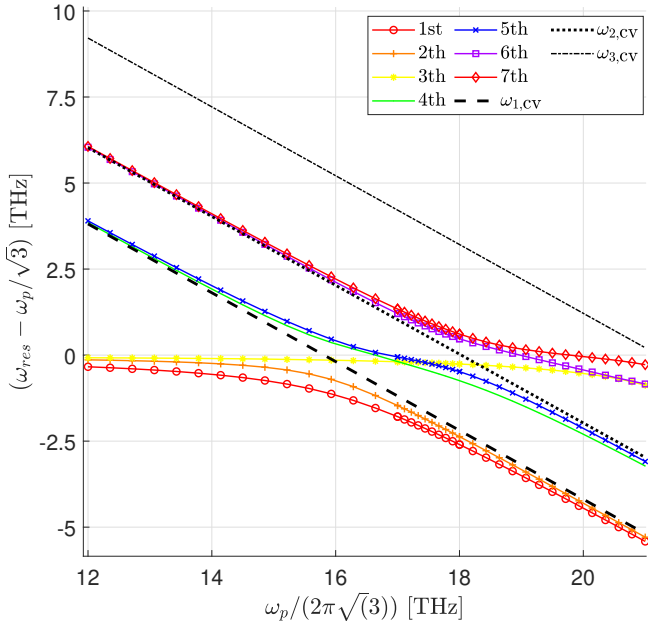


FIG. 5. Change of the lower resonance frequencies as a function of the isolated particle's resonance frequency ( $\omega_p/\sqrt{3}$ ) or, equivalently, as a function of the plasma frequency ( $\omega_p$ ).  $\omega_{i,cv}$  denote the  $i$ -th cavity resonance frequency

modes. We distinguish between two families of resonant frequencies. The first family, entitled *cavity/particle* consists of the first three resonances (see the numbering scheme in the legend of Fig. 5). We qualify them as particle's resonances that are affected by the cavity loading. Note that these exist already below the cutoff of the first resonance in the isolated cavity. In addition, the first two resonance frequencies are excited by the TE-mode field while the third is excited by a z-polarised field. As the plasma frequency is increased, the former two resonances converge to the first cavity resonant frequencies (lowest black-dashed line) whereas the latter is only slightly affected by the increase in the plasma frequency.

The rest of the resonance frequencies constitute the second family entitled *particle/cavity*, shown in Fig. 5. We qualify them as the influence of the particle on the cavity. They originate around one of the cavity resonance frequencies and migrate towards the following one, as the plasma frequency of the particle is increasing. It is important to acknowledge that the transition from one cavity cutoff to the next would be hard to apprehend using a perturbation theory.

## B. Analysis of the dynamics of a gyrotropic particle inside the cavity

### 1. Problem description

A more complex problem consists of a gyrotropic plasmonic particle inside the cavity and subject to an external static biasing magnetic field  $\mathbf{B}_0 = \hat{z}B_0$ . We assume that the particle has a volume  $V$ , and its radius is much smaller than any of the cavity's dimensions so that we can still use the dipole approximation. Such a particle can be modeled using a relative permittivity conformed to the Drude Model. The dynamic polarizability matrix of the particle that includes the radiation loss can be obtained from its relative permeability tensor [47, 48] and expressed as follows,

$$\underline{\underline{\alpha}}^{-1} = \underline{\underline{\alpha}}_e^{-1} = \frac{k^3}{6\pi\varepsilon} \left( \underline{\underline{\alpha}}_h^{-1} + j\underline{\underline{I}} \right) \quad (33)$$

$$\underline{\underline{\alpha_h}}^{-1} = \begin{bmatrix} g_{xx} & -jg_{xy} & 0 \\ jg_{xy} & g_{yy} & 0 \\ 0 & 0 & g_{zz} \end{bmatrix} \quad (34a)$$

with

$$g_{uu} = \left( \frac{6\pi}{k^3 V} \right) \left( \frac{1}{3} - \frac{(\omega - j\gamma)\omega}{\omega_p^2} \cdot \frac{(\omega - j\gamma)^2 - \omega_c^2}{(\omega - j\gamma)^2 + \omega_c^2} \right) \quad (34b)$$

$$g_{zz} = \left( \frac{6\pi}{k^3 V} \right) \left( \frac{1}{3} - \frac{(\omega - j\gamma)\omega}{\omega_p^2} \right) \quad (34c)$$

$$g_{xy} = \left( \frac{6\pi}{k^3 V} \right) \left[ \frac{(\omega - j\gamma)\omega_c}{\omega_p^2} \cdot \frac{(\omega - j\gamma)^2 - \omega_c^2}{(\omega - j\gamma)^2 + \omega_c^2} \right. \\ \left. - \frac{2}{3} \frac{\omega_c(\omega - j\gamma)}{(\omega - j\gamma)^2 + \omega_c^2} \right] \quad (34d)$$

where  $\omega_p$ ,  $\omega_c = -q_e B_0 / m_e$ , and  $\gamma$  denote the plasma, cyclotron, and collision frequencies, respectively.

The resonance frequency of the isolated gyrotrropic particle can be obtained by setting  $\det(\underline{\underline{\alpha}}^{-1}) = 0$ . This leads to a quite complicated analytical expression. A rather intuitive and approximated results can be obtained under two separate assumptions:  $\omega$  and  $\omega_c \ll \omega_p$  and  $\omega \gg \omega_c$

For  $\omega$  and  $\omega_c \ll \omega_p$  and  $\gamma = 0$  for lossless particle,

$$g_{uu} = g_{zz} = \frac{1}{3} \left( \frac{6\pi}{k^3 V} \right) \quad (35a)$$

$$g_{xy} = -\frac{2}{3} \left( \frac{6\pi}{k^3 V} \right) \frac{\omega \omega_c}{\omega^2 + \omega_c^2} \quad (35b)$$

which yields a resonance at  $\omega_0 = \omega_c$ . It can easily be shown that this frequency has two degenerative eigenstates with right-hand circular polarization (RHCP) and left-hand-circular polarization (LHCP), respectively. Using a numerical approach, we find that although the exact resonant frequencies occur around  $\omega_c$  and the polarization of the eigenstates is exactly as obtained analytically, they are non-degenerative.

For  $\omega \gg \omega_c$  and  $\gamma = 0$  for lossless particle, we get the familiar expressions [49]:

$$g_{uu} = g_{zz} = \left( \frac{6\pi}{k^3 V} \right) \left( \frac{1}{3} - \frac{\omega^2}{\omega_p^2} \right) \quad (36a)$$

$$g_{xy} = \left( \frac{6\pi}{k^3 V} \right) \frac{\omega \omega_c}{\omega_p^2} \quad (36b)$$

that yields the following three resonance frequencies:

$$\omega_{\pm} = \frac{\omega_p}{\sqrt{3}} \sqrt{1 + \frac{3}{4} \frac{\omega_c^2}{\omega_p^2} \pm \frac{\omega_c}{2}}, \omega'_0 = \frac{\omega_p}{\sqrt{3}}. \quad (37)$$

Obviously, the first two resonances correspond to excitation perpendicular to the magnetization in the  $xy$  plane, while the last one, which is identical to the resonance frequency in the absence of magnetization, corresponds to excitation along the  $z$  axis, that is not affected by the materials gyrotropy. In the following we

see how the different types of cavity modes E-modes and H-modes differently affect the coupling between the the resonances of the isolated particle in the  $xy$  plane and along  $z$ .

## 2. Results and Insights

We analyzed the influence of the plasmonic frequency on the coupled system, for a fixed cyclotron frequency,  $\omega_c$ . We targeted to have the cavity resonant frequencies near  $\omega_p/\sqrt{3}$  which is at the resonance frequency of the particle when isolated and with  $\omega_c = 0$  (see Eq. (37)) for effective coupling. This, however, implies that the resonance of the particle near  $\omega_c$  is far below the cavity's first resonance and thus weakly affected by the coupling.

In general, except for the presence of two resonant frequencies near  $\omega_c$  due to the particle, the migrations of the resonance frequencies follow the same trend as in the case of the unmagnetized isotropic particle (see Fig. 5). Consider first Fig. 6. It shows the migration of the resonance frequencies with respect to the increase in the plasma frequency. In the four sub-figures (a)-(d), we see the effect for different but fixed cyclotron frequencies: (a)  $\omega_c/2\pi = 0.3\text{THz}$ , (b)  $\omega_c/2\pi = 1.2\text{THz}$ , (c)  $\omega_c/2\pi = 2.1\text{THz}$ , and (d)  $\omega_c/2\pi = 3\text{THz}$ . As we increase  $\omega_c$ , the *particle/cavity*, namely, what we consider as the cavity resonances that are affected by the particle, respond differently to the increase in the cyclotron frequency. Specifically, the degenerate resonance pairs #4-#5, and #6-#7 are split in a way that emerges a "eye" shape in the dispersion diagrams around the plasma frequency of the isolated unmagnetized particle. As  $\omega_c$  increases, the "eye" further opens.

As expected, the biasing of the magnetic field along the  $\hat{z}$  axis, leaves the frequency associated with the excited dipole in the  $\hat{z}$  axis (the brown line in Fig. 6(a) that corresponds to the 2nd resonance) is barely changed by the change in the biasing field. However, spacing between the other two resonance frequencies (1st and 3rd) *cavity/particle* increases with the cyclotron frequencies. This can also be considered as an "eye" that opens around  $\omega_p = 0$ .

The investigation of the effect of the cyclotron frequency on the system, for fixed  $\omega_p$ , provides a different interesting perspective. We focus on the  $\omega_c \ll \omega_p$  case. For fixed plasma frequency, and  $\omega_c \ll \omega_p$ , we can obtain using a first-order Taylor approximation applied on Eq. (37) that the resonant frequencies for the isolated particle are linear in the cyclotron frequency.

$$\omega_{\pm} = \left( \frac{\omega_p}{\sqrt{3}} \pm \frac{\omega_c}{2} \right) + \frac{\sqrt{3}}{8} \frac{\omega_c^2}{\omega_p} \quad \omega_0 = \frac{\omega_p}{\sqrt{3}}. \quad (38)$$

When inserted in the cavity, the empty cavity resonance frequencies constitute bound levels for the coupled system, in the sense that when a resonance occurs below or above a cavity resonance, it stays below

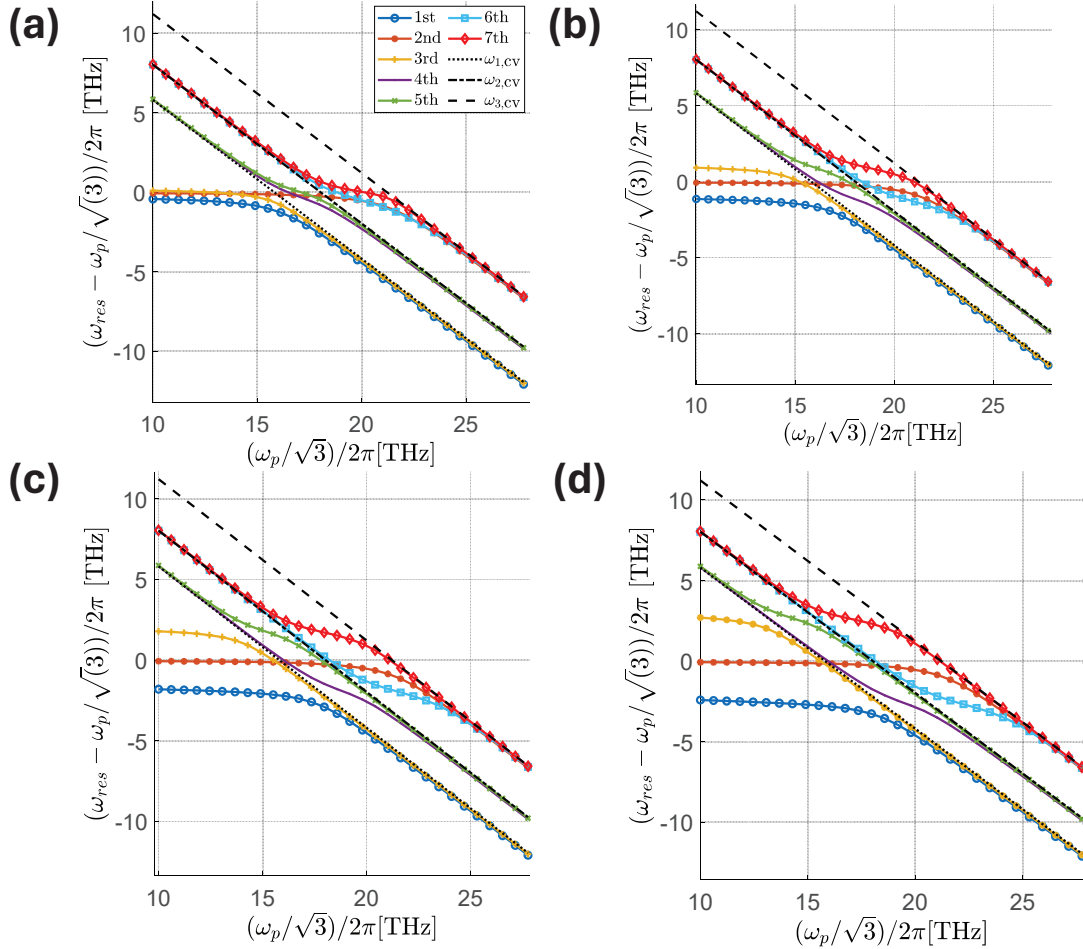


FIG. 6. Change of the lower resonance frequencies as a function of particle's plasma frequency ( $\omega_p$ ), while the amplitude of the bias magnetic field is kept constant.  $\omega_{i, cv}$  denote the  $i$ -th cavity cutoff frequency. (a) The cyclotron frequency ( $\omega_c/2\pi$ ) = 0.3 THz. (b)  $\omega_c/2\pi$  = 1.2 THz. (c)  $\omega_c/2\pi$  = 2.1 THz. (d)  $\omega_c/2\pi$  = 3 THz.

or above it. As shown in Fig. 6 (a-d) that corresponds to  $\omega_p/2\pi = 12, 14, 15.2, 16$  THz, respectively. We may again identify the first three resonances as *cavity/particle* resonances. The first and second resonance frequencies follow a trend analogous to the isolated particle case. In contrast, the third frequency does not cross the first cutoff frequency of the cavity  $\omega_{1, cv}$ , thus preventing it from following the trends of the isolated case, for high plasmonic frequencies. However, increasing plasmonic frequencies dictates how fast it converges to  $\omega_{1, cv}$ .

### C. Analysis of the dynamics of a Chiral particle inside the cavity

#### 1. Problem description

As we already demonstrated with the proper definition of the polarizability of a given material, provided the DDA's assumption holds, we can obtain a detailed resonance behavior. Here we focus on a small resonating

object with chiral (biisotropic) properties. A point-like chiral sphere of volume  $V$  can be described by dynamic polarizability tensor, which is a transition matrix that linearly maps the incident field to the excited moments as [50, 51]:

$$\begin{bmatrix} \mathbf{p} \\ \mathbf{m} \end{bmatrix} = \underline{\underline{\alpha}} \begin{bmatrix} \mathbf{E}_{\text{inc}}(\mathbf{r}', \mathbf{r}') \\ \mathbf{H}_{\text{inc}}(\mathbf{r}', \mathbf{r}') \end{bmatrix} \quad (39)$$

where  $\mathbf{p}, \mathbf{m}$  denote the induced electric dipole moment and magnetic moment, respectively and  $\mathbf{E}_{\text{inc}}$  and  $\mathbf{H}_{\text{inc}}$  are the incident electric and magnetic field, respectively.

Here as well, to obtain the dynamic polarizability, the quasi-static polarizability  $\underline{\underline{\alpha}}_s$  is corrected for energy conservation:

$$\underline{\underline{\alpha}}^{-1} = \underline{\underline{\alpha}}_s^{-1} + \begin{bmatrix} j \frac{k^3}{6\pi\varepsilon_0} \underline{\underline{I}} & \underline{\underline{0}} \\ \underline{\underline{0}} & j \frac{k^3}{6\pi\mu_0} \underline{\underline{I}} \end{bmatrix} \quad (40a)$$

$$\underline{\underline{\alpha}}_s = \begin{bmatrix} \underline{\underline{\alpha}}_{ee} & -j \underline{\underline{\alpha}}_{em} \\ j \underline{\underline{\alpha}}_{em}^T & \underline{\underline{\alpha}}_{mm} \end{bmatrix} \quad (40b)$$

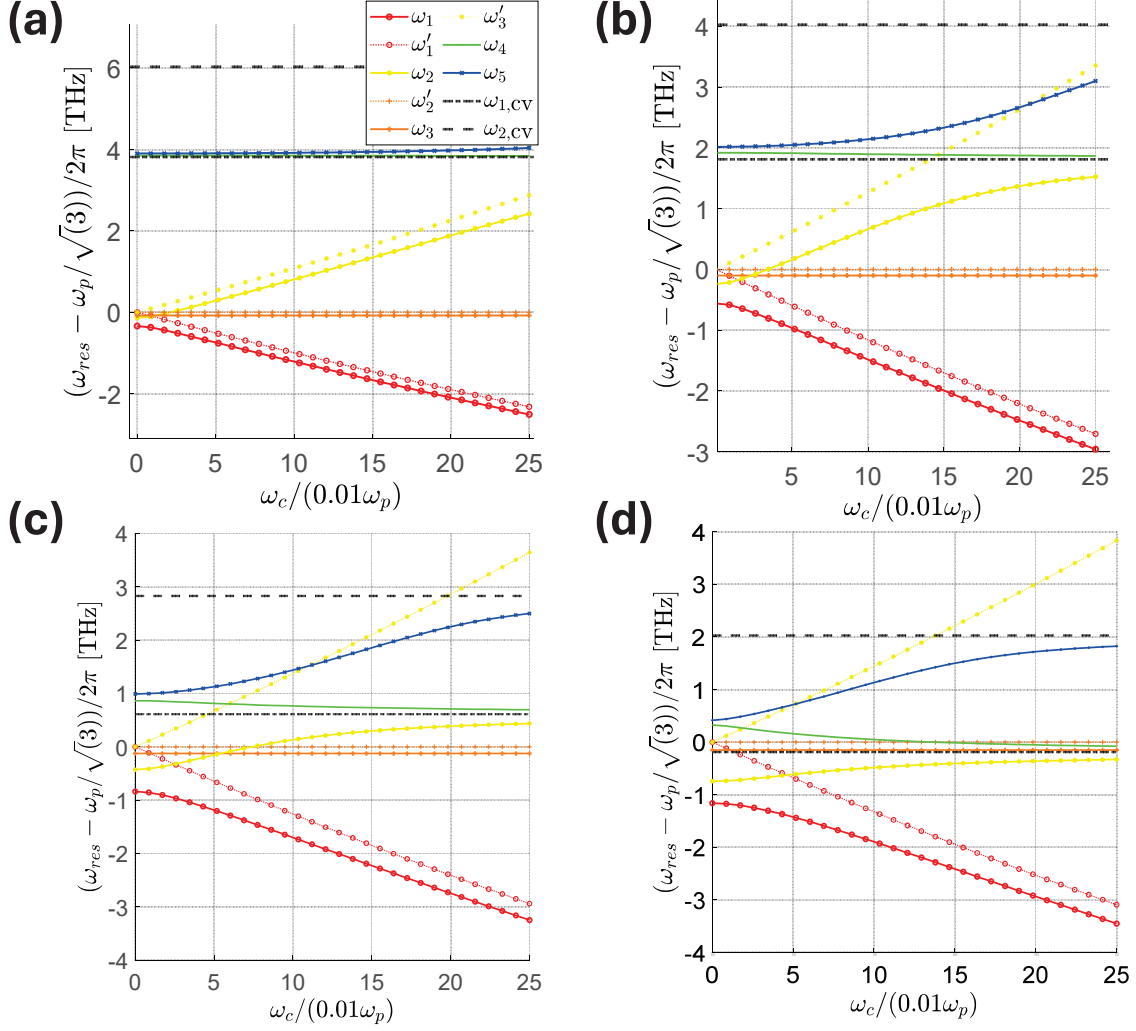


FIG. 7. Change of the lower resonance frequencies as a function of particle's cyclotron frequency ( $\omega_c$ ). Now, the material's plasma frequency  $\omega_p$  is different but fixed.  $\omega_{i,\text{cv}}$  denote the  $i$ -th cavity cutoff frequency.  $\omega'_i$  denote the  $i$ -th resonance frequency of the isolated gyrotrropic particle. (a) for  $(\omega_p/2\pi) = 12\text{THz}$ . (b) for  $\omega_p/2\pi = 14\text{THz}$ . (c) for  $\omega_p/2\pi = 15.2\text{THz}$ . (d) for  $\omega_p/2\pi = 16\text{THz}$ .

where  $\varepsilon_0$  is the vacuum permittivity and  $\mu_0$  is the permeability of free space;  $\underline{\underline{0}}$  stands for the  $3 \times 3$  zero-matrix. The electric, magnetic, and mixed electric-magnetic dipole polarizabilities  $\underline{\underline{\alpha}}_{ee}$ ,  $\underline{\underline{\alpha}}_{mm}$ ,  $\underline{\underline{\alpha}}_{em}$  are expressed as below,

$$\underline{\underline{\alpha}}_{ee} = 3\varepsilon_0 V \frac{(\varepsilon_r(\omega) - 1)(\mu_r(\omega) + 2) - \kappa^2}{(\varepsilon_r(\omega) + 2)(\mu_r(\omega) + 2) - \kappa^2} \underline{\underline{I}} \quad (41\text{a})$$

$$\underline{\underline{\alpha}}_{mm} = 3\mu_0 V \frac{(\varepsilon_r(\omega) + 2)(\mu_r(\omega) - 1) - \kappa^2}{(\varepsilon_r(\omega) + 2)(\mu_r(\omega) + 2) - \kappa^2} \underline{\underline{I}} \quad (41\text{b})$$

$$\underline{\underline{\alpha}}_{em} = \frac{V}{\eta} \frac{9\kappa}{(\varepsilon_r(\omega) + 2)(\mu_r(\omega) + 2) - \kappa^2} \underline{\underline{I}} \quad (41\text{c})$$

where  $\underline{\underline{I}}$  is the  $3 \times 3$  identity matrix;  $\eta$  is the intrinsic impedance of a medium;  $\kappa$  is the chiral parameter, and the relative permittivity  $\varepsilon_r$  and permeability  $\mu_r$  are defined according to the Drude model and the Lorentz

model respectively and read:

$$\varepsilon_r(\omega) = 1 - \frac{\omega_p}{\omega^2} \quad (42\text{a})$$

$$\mu_r(\omega) = 1 + \frac{F\omega_0}{\omega_0^2 - \omega^2} \quad (42\text{b})$$

where  $\omega_p, \omega_0$  are the plasma and the resonant frequencies respectively. We assume no loss in the particle.  $\mu_r$  coincide with the effective response of an array of (splitting resonators) SRR, with array parameter  $F$  [52–54] whereas  $\varepsilon_r$  would describe the effective dielectric permittivity of a thin wire medium [54].

When placed inside the cavity, we substitute  $\underline{\underline{\alpha}}$  with

$\underline{\underline{\alpha}}_{\text{eff}}$  which reads,

$$\underline{\underline{\alpha}}_{\text{eff}}^{-1} = \left[ \underline{\underline{\alpha}}^{-1} - \begin{pmatrix} \underline{\underline{G}}_{ee}^s & \underline{\underline{G}}_{em}^s \\ \underline{\underline{G}}_{em}^s & \underline{\underline{G}}_{mm}^s \end{pmatrix} \right] \quad (43)$$

where  $\underline{\underline{G}}^s(\mathbf{r}', \mathbf{r}')$  represent the complete local Dyadic Green's function inside the cavity, obtained in Sec. IV, as well as in App. C. Finally, the resonance of this new coupled system is obtained by searching for frequencies that will nullify the determinant of the  $\underline{\underline{\alpha}}_{\text{eff}}$  in Eq. (43).

## 2. Results and Insights

Similarly to previous examples, we investigated the effect of the plasmonic frequencies on the coupled system. We analyze three cases with  $\kappa = 0$ ,  $\kappa = 0.4$ , and  $\kappa = 2$  while fixing the resonance frequency parameter  $\omega_0 = 17\text{THz}$ , and  $F=0.6$ . Throughout the analysis, we distinguish again between the two families of resonances. *cavity/particle* consists of two parts,  $P_1, P_2$  where the former groups the first three resonances, and the latter groups of either the last three solutions for Fig. 8(a)) or the last five (Fig. 8(b-c)) solutions. More details are provided below. The second family *particle/cavity* is also divided in two,  $CV_1$  consisting of  $\omega_4, \omega_5$ ;  $CV_2$  consisting of  $\omega_6, \omega_7$ . (Fig. 8(a-c)).

For  $\kappa = 0$ , the isolated particle has two resonance frequencies

$$\omega_e = \frac{\omega_p}{\sqrt{3}} \quad (44)$$

$$\omega_m = \omega_0 \sqrt{\frac{3}{3 - F}} \quad (45)$$

At the resonance  $\omega_e$ , only the electric dipole is excited, and at  $\omega_m$ , only the magnetic moment is excited. Each has three degenerative states due to spherical symmetry. When embedded in the cavity, the cavity mediates the coupling between the electric dipole and the magnetic moment, and the resulting resonance frequencies are depicted in Fig. 8(a). In general, as demonstrated so far, the coupling of the particle to the cavity breaks the degeneracy in the system. For low plasmonic frequency  $\omega_p$ ,  $CV_1$  and  $CV_2$  occur near the first  $\omega_{1,\text{cv}}$  and second  $\omega_{2,\text{cv}}$  (empty) cavity resonance, respectively and their dynamics as a function of increasing  $\omega_p$  is similar to the isotropic case (Fig. 5). Moreover, the resonance  $P_1$  and  $P_2$  occurs near  $\omega_e$  (horizontal dash line) and  $\omega_m$  (slanted dash line) respectively. On one hand, The migration of  $P_1$  is similar to when the particle was isotropic and modeled by a simple electric dipole (Fig. 5), with the main difference that the 3rd resonance (yellow line) associated with the dipole in  $\hat{z}$  axis migrates towards the  $\omega_m$ , as  $\omega_p$  increases and for  $\omega_p > \omega_0\sqrt{3}$ ). In the other, in the  $P_2$

group, only the resonance associated initially with the magnetic moment excited in  $\hat{z}$  axis is strongly affected, and hereby migrates to the third cutoff  $\omega_{3,\text{cv}}$ . This behavior is analogous to one of the first two resonances in  $P_1$ . Importantly, each of the remaining two resonances is degenerative with two states due to the inherited degeneracy in the cavity ( $a = b$ ).

For  $\kappa > 0$ , the isolated particle resonates predominantly as a magnetic moment. Although the particle exhibits two resonance frequencies, with  $\omega_m$  one of its asymptotic values ( for  $\kappa = 0.6$ ,  $\omega_e$  remains an asymptote) the curves of the frequencies with respect to  $\omega_p$  do not cross, and the gap between the curves increases with  $\kappa$ . In the coupled system, the dynamics of  $P_1$ 's and  $CV_1$ 's frequencies follow a similar trend as in  $\kappa = 0$  case. Further, for both  $\kappa = 0.4$  and  $\kappa = 2$ , the strong coupling of the excited magnetic moment to the cavity kept  $CV_2$ 's frequencies confined as they are led from the frequencies from  $\omega_{2,\text{cv}}$  towards  $\omega_m$ . Concerning  $P_2$ 's frequency, we observe two interesting outcomes: first, the coupling breaks the cavity imposed degeneracy noted in the case of  $\kappa = 0$  therefore there is a total of five non-degenerative modes in  $P_2$ . Second, there is a gap between the  $P_2$  and  $CV_2$ , similar to the one between the resonance of the isolated particle. For  $\kappa = 0.4$ , the  $P_2$ 's frequencies migrate from the  $\omega_m$  towards the 3rd cavity resonance frequency while for  $\kappa = 2$ , they are mostly confined near the third cavity resonance frequency due to the increased gap.

## VI. CONCLUSION

In this paper, we explored the mutual dynamics between a resonant particle and a cavity using the discrete dipole approximation and polarizability theory. The two main contributions of the paper are (i) the introduction of an exact, semi-analytical, approach that is numerically robust and computationally efficient for the calculation of the local field that acts on the particle's polarizability in the dipole induction process. Using this approach, one can directly use known polarizabilities with a simple and standard free-space radiation correction term in order to solve for the collective excitation. In a broader sense, we suggest a ladder-type singularity subtraction approach that may be used in even more complicated scenarios when the modal decomposition cannot be performed analytically, but instead, the modal functions should be found numerically. In these cases, other alternative approaches, such as the use of the Ewald summation technique or image theory, are not applicable to begin with, while the suggested ladder-type subtraction methodology still holds. (ii) As an additional contribution, we explore the physics of the collective excitation of the resonant (here plasmonic) particle in the cavity. We identify two families of resonances. Resonances that can be considered as particle resonances affected by the cavity loading, and cavity resonances that are affected by the particle loading. This mutual loading breaks the modal degener-

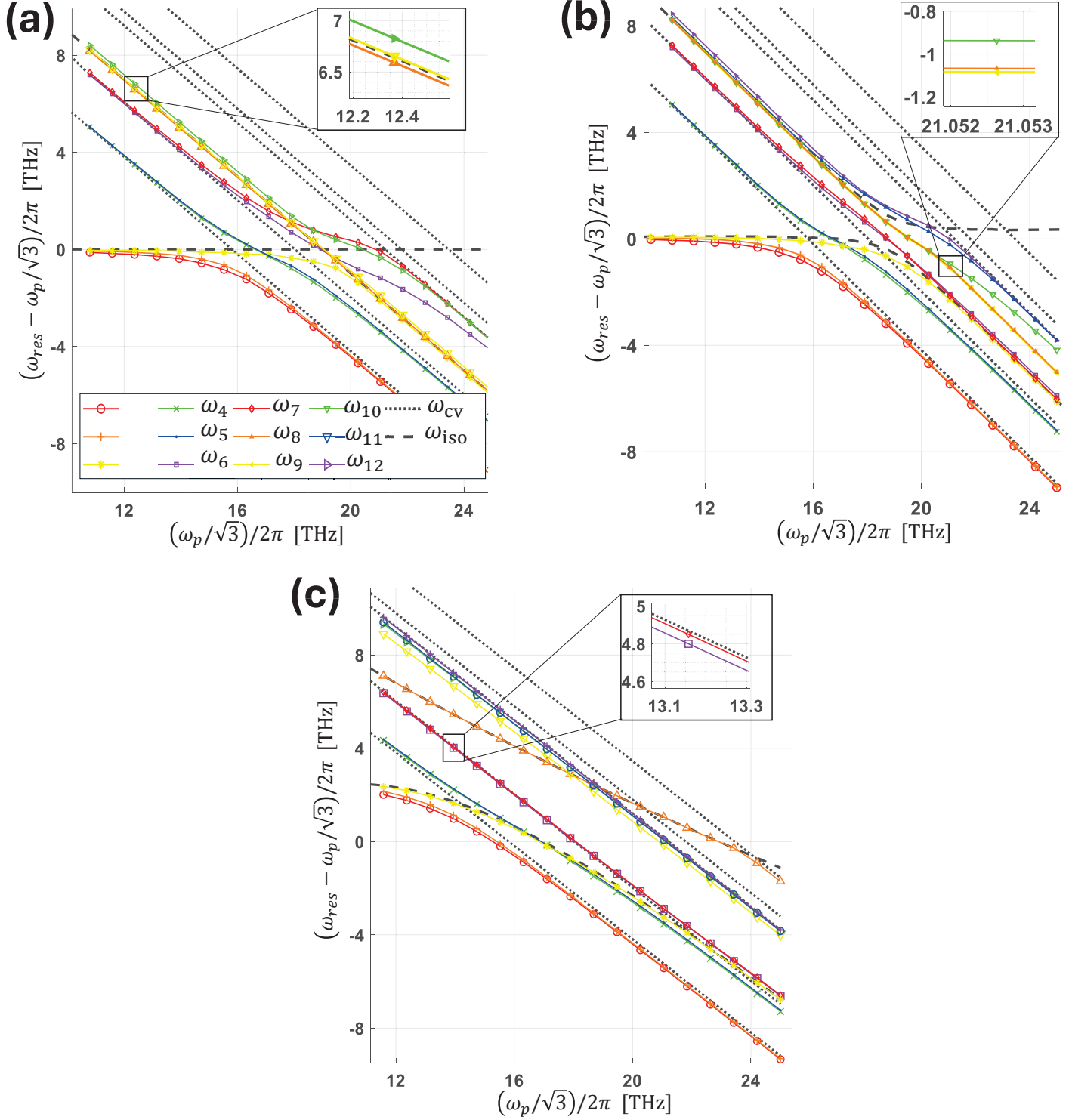


FIG. 8. Change of the lower resonance frequencies as a function of particle's plasma frequency ( $\omega_p$ ), while the chiral parameter  $\kappa$  is kept constant.  $F = 0.6$ ,  $\omega_0/2\pi = 17$  THz  $\omega_{cv}$  (dotted lines) denote the empty cavity resonance frequencies, whereas  $\omega_{iso}$  (dash lines) are the particle's resonance when isolated. (a)  $\kappa = 0$ : the horizontal and slanted dash line represent  $\omega_e$  and  $\omega_m$  respectively (b)  $\kappa = 0.4$  (c)  $\kappa = 2$

acy that is present in each of the isolated sub-systems, the particle and the cavity. In addition, we demonstrate that our approach can be used to explore the collective dynamics when more complex polarizability is considered, such as for a chiral particle and (magnetized) gyrotropic particle. In an accompanying work [48], we focus further on this later problem and demonstrate the unique magnetization-loss threshold phenomenon that originates when exploring Lorentz (non-)reciprocity in the space of cyclotron frequency and the plasma damping coefficient in this system.

### ACKNOWLEDGMENTS

This research was supported by the Israel Science Foundation (Grant No. 1457/23).

The authors would like to thank Profs. Vitaliy Lomakin and Sergei Tretyakov for useful discussions and critical comments.

### Appendix A: Green's Function Formalism

For the sake of completeness, in this section, we provide the basic formulation and underlying ideas of developing the Dyadic Green's function in a bounded medium with a uniform cross-section along one of the axes. The formalism is taken as is from Chapters 2 and 3 of Felsen & Marcuvitz's Book [46].

We present the formalism assuming an infinitesimal electric or magnetic current source at  $\mathbf{r}'$ , oriented in  $\hat{\mathbf{z}}$  and we obtain the expression of the electromagnetic fields  $\mathbf{E}(\mathbf{r}, \mathbf{r}')$ ,  $\mathbf{H}(\mathbf{r}, \mathbf{r}')$  at any point  $\mathbf{r}$  inside the domain of interest. The steady-state electromagnetic fields excited by a specific electric current distribution  $\mathbf{J}(\mathbf{r})$  and magnetic current distribution  $\mathbf{M}(\mathbf{r})$  are respect Maxwell's equations,

$$\nabla \times \mathbf{E}(\mathbf{r}) = -j\omega\mu\mathbf{H}(\mathbf{r}) - \mathbf{M}(\mathbf{r}) \quad (A1a)$$

$$\nabla \times \mathbf{H}(\mathbf{r}) = j\omega\epsilon\mathbf{E}(\mathbf{r}) + \mathbf{J}(\mathbf{r}) \quad (A1b)$$

$$\nabla \cdot \epsilon\mathbf{E}(\mathbf{r}) = 0 \quad (A1c)$$

$$\nabla \cdot \mu\mathbf{H}(\mathbf{r}) = 0 \quad (A1d)$$

$$(A1e)$$

We choose the  $z$ -axis as the direction of propagation and we decompose the electric and magnetic field in transverse and longitudinal components. The longitudinal components can be expressed based on the transverse components so we focus on the latter. The transversal cross-section of the bounded media is assumed to be uniform. We denote  $(\mathbf{e}_i, \mathbf{h}_i)$  the eigenmode vector fields yield by boundary value problem in the transversal plane. It can be proven that they form a complete orthonormal basis set [36],[46].

The transversal boundary problem can be written in terms of scalar potentials as follows:

For **E-modes**

$$\begin{aligned} \nabla_t^2 \Phi_i + k'_{t,i} \Phi_i &= 0 \text{ in } S \\ \begin{cases} \Phi_i = 0 \text{ on } \delta S \text{ if } k'_{t,i} \neq 0 \\ \frac{\partial \Phi_i}{\partial s} = 0 \text{ on } \delta S \text{ if } k'_{t,i} = 0 \end{cases} \end{aligned} \quad (A2)$$

For **H-modes**

$$\begin{aligned} \nabla_t^2 \Psi_i + k''_{t,i} \Psi_i &= 0 \text{ in } S \\ \frac{\partial \Psi_i}{\partial s} &= 0 \text{ on } \delta S \end{aligned} \quad (A3)$$

The resulting eigenmode vector fields are obtained as follows.

$$\mathbf{e}'_i(\rho) = -\frac{\nabla_t \Phi_i}{k'_{t,i}} \quad (A4a)$$

$$\mathbf{e}''_i(\rho) = -\frac{\nabla_t \Psi_i}{k''_{t,i}} \times \hat{\mathbf{z}} \quad (A4b)$$

$$\mathbf{h}'_i(\rho) = -\hat{z} \times \frac{\nabla_t \Phi_i}{k'_{t,i}} \quad (\text{A5a})$$

$$\mathbf{h}''_i(\rho) = -\frac{\nabla_t \Psi_i}{k'_{t,i}} \quad (\text{A5b})$$

Here  $\hat{z}$  represents the longitudinal unit vector,  $S$  is the interior of the guiding structure, and  $\delta S$  is its boundary.

The decomposition of the sources in our modal basis yields the amplitudes  $v_i(z)$  and  $i_i(z)$  that are given in Eq. (A6a) and Eq. (A6b). As the equations are identical for both E- and H-modes, the prime and double prime are omitted.

$$v_i(z) = Z_i^* \iint_S \mathbf{J}(r) \cdot \mathbf{e}_{z,i}^*(\rho) dS + \iint_S \mathbf{M}(r) \cdot \mathbf{h}_i^* dS \quad (\text{A6a})$$

$$i_i(z) = \iint_S \mathbf{J}(r) \cdot \mathbf{e}_i^* dS + Y_i^* \iint_S \mathbf{M}(r) \cdot \mathbf{h}_{z,i}^*(\rho) dS \quad (\text{A6b})$$

where

$$\mathbf{e}'_{z,i} = \hat{z} \frac{\nabla_t \cdot \mathbf{e}_i'(\rho)}{Z_i' j \omega \varepsilon} \text{ and } \mathbf{e}''_{z,i} = 0 \quad (\text{A7a})$$

$$\mathbf{h}'_{z,i} = 0 \text{ and } \mathbf{h}''_{z,i} = \hat{z} \frac{\nabla_t \cdot \mathbf{h}_i'(\rho)}{Y_i'' j \omega \mu} \quad (\text{A7b})$$

Thus, the excited fields are represented below [46].

$$\mathbf{E}_t(r) = \sum_i V_i'(z) \mathbf{e}_i'(\rho) + \sum_i V_i''(z) \mathbf{e}_i''(\rho) \quad (\text{A8a})$$

$$\mathbf{H}_t(r) = \sum_i I_i'(z) \mathbf{h}_i'(\rho) + \sum_i I_i''(z) \mathbf{h}_i''(\rho) \quad (\text{A8b})$$

$$j \omega \varepsilon E_z(r) + J_z(r) = \sum_i I_i'(z) \nabla_t \cdot \mathbf{e}_i'(\rho) \quad (\text{A8c})$$

$$j \omega \mu H_z(r) + M_z(r) = \sum_i V_i''(z) \nabla_t \cdot \mathbf{h}_i''(\rho) \quad (\text{A8d})$$

Where  $\mathbf{E}_t, \mathbf{H}_t$  represent the transverse component Electrical and Magnetic fields, respectively.  $E_z, H_z$  represent the longitudinal component of the electric and magnetic fields, respectively, and  $J_z, M_z$  represent the longitudinal component of electric and magnetic sources.

Finding the amplitudes  $V_i(z)$  and  $I_i(z)$  subject to the boundary conditions in the longitudinal axis is equivalent to obtaining the voltage and current amplitude, respectively, along a 1D transmission lines (TL) that models the longitudinal modal behavior (here along the  $z$ -axis) with modal sources  $v_i(z)$  and  $i_i(z)$ . For uniform medium (except for boundaries), the TL model has the

uniform (along  $z$ ) propagation constant  $\kappa$  and characteristic impedance  $Z'$  or  $Z''$  which is polarization and mode dependent. These are given by,

$$\kappa = \sqrt{k^2 - k_{t,i}^2} \text{ with } \text{Im}\{\kappa\} > 0 \quad (\text{A9})$$

satisfying the radiation condition, and

$$Z' = \kappa / \omega \varepsilon \quad (\text{E-mode}) \quad (\text{A10a})$$

$$Z'' = \omega \mu / \kappa \quad (\text{H-mode}). \quad (\text{A10b})$$

## Appendix B: Illustration of resulting eigenmode expansions

The local Green's function can be expressed as:

$$\begin{aligned} \mathbf{G}^s = & \underbrace{\sum_{\text{1D-finite}} \sum_{\text{CV}}}_{\mathbf{G}_{\text{CV}}} - \underbrace{\sum_{\text{1D-inf}} \sum_{\text{RG1}}}_{\mathbf{G}_{\text{RG1}}} \\ & + \underbrace{\sum_{\text{1D-finite}} \int_{\text{RG2}}}_{\mathbf{G}_{\text{RG2}}} - \underbrace{\sum_{\text{1D-inf}} \int_{\text{PP1}}}_{\mathbf{G}_{\text{PP1}}} \\ & + \underbrace{\sum_{\text{1D-finite}} \iint_{\text{PP2}}}_{\mathbf{G}_{\text{PP2}}} - \underbrace{\sum_{\text{1D-inf}} \iint_{\text{FS}}}_{\mathbf{G}_{\text{FS}}} \end{aligned} \quad (\text{B1})$$

where the local dependence  $r'$  is omitted and each term is expressed in the format  $\underbrace{zzz}_{yyy} \underbrace{xxx}_{xxx}$  should be interpreted as

follows:  $xxx$  symbolize the bounded medium type,  $yyy$  represents the type of expression from the eigenmode expansion in "transverse" plane, and  $zzz$  denotes the form of the resulting 1D TL problem. The TL problem are either infinite in the longitudinal axis denoted by 1D – inf or finite denoted by 1D – finite.  $\mathbf{G}_{\text{RG1}}$  and  $\mathbf{G}_{\text{RG2}}$  are the two equivalent alternative representations of Green's function in the RGW.  $\mathbf{G}_{\text{PP1}}$  and  $\mathbf{G}_{\text{PP2}}$  are the two equivalent alternative representations of Green's function inside infinite parallel plates waveguide.

## Appendix C: Local electric and magnetic Green's Function due to a magnetic current element with $\mathbf{M} = \delta(\mathbf{r} - \mathbf{r}')\hat{z}$

We present below a summary of the final expression needed to calculate the local field for a *magnetic* current source along the  $\hat{z}$  direction. We set  $M_0 = 1[\text{Vm}]$ .

In essence, the procedure described compactly by Eq. (11b) holds also for this case, and the idea behind each line in the subtraction as presented through Sec. ( III A) still stands. For each case (cavity, RG1, RG2, PP1, PP2 or free-space), one uses the same longitudinal axis and use the same eigenmode  $\{\mathbf{e}_i'(\rho), \mathbf{h}_i'(\rho), \mathbf{e}_i''(\rho), \mathbf{h}_i''(\rho)\}$ . The fields can be expressed using (A8a-A8d) for  $J_z = 0$  and  $M_z = \hat{z} \delta(\mathbf{r} - \mathbf{r}')$ . The key difference resides in the modal voltage and current sources in the 1D TL problems which depend intrinsically

on the physical sources in the bounded domain as indicated by Eqs. (A6a)-(A6b). Unless stated explicitly otherwise, the TL model for E- and H-modes are the same, except for the specific expression for the characteristic impedance  $Z_i$  that varies between the polarizations and the modes.

a. *Cavity Green's function and the first form of infinite Rectangular Waveguide's Green's Function*

Similarly to Sec. III A.1, the transverse eigenvectors for E-mode and H-mode problems are obtained from the scalar potentials expressed in Eqs. (12,13). For the longitudinal problem of the 1D TL along the  $z$ -axis, the sketch (Fig. 2 (b),(d)) is identical up to the sources: namely, in the cavity case the TL is shorted at its terminations, while in the rectangular waveguide case the TLs are infinite. In contrast, the sources in the TL problem, obtained according to Eqs. (A6a),(A6b) reads, for E-mode

$$v_i(z; \mathbf{r}') = 0, \quad i_i(z; \mathbf{r}') = 0 \quad (\text{C1})$$

while for H-mode

$$v_i(z; \mathbf{r}') = 0 \quad (\text{C2})$$

$$i_i(z, \mathbf{r}') = j \frac{k'_{t,i}}{\omega \mu} \sqrt{\frac{\epsilon_n \epsilon_m}{ab}} \cos\left(\frac{m\pi x'}{a}\right) \cos\left(\frac{n\pi y'}{b}\right) \delta(z-z') \quad (\text{C3})$$

with  $k_{t,i}^2 = (\frac{m\pi}{a})^2 + (\frac{n\pi}{b})^2$  and  $0 \leq n, m \leq \infty$ , and  $i$  denote a double indexing  $(n, m)$ ;  $\epsilon_l = 2 - \delta[l]$  for  $l = n, m$  and here also  $\delta[\cdot]$  denotes Kronecker's delta function.

As expected, with this decomposition, only H-modes are excited inside the cavity. Now the TL problem can be readily solved for the cavity,

$$\begin{aligned} \mathcal{V}_{\text{CV},i}(z, z') &= \frac{Z_i}{2(e^{-2j\kappa c} - 1)} (e^{-j\kappa|z-z'|} \\ &- e^{-j\kappa(z+z')} - e^{-j\kappa(2c-(z+z'))} + e^{-j\kappa(2c-|z-z'|)}) \end{aligned} \quad (\text{C4a})$$

$$\begin{aligned} \mathcal{I}_{\text{CV},i}(z, z') &= \frac{1}{2(e^{-2j\kappa c} - 1)} (\varsigma_{z,z'} \cdot e^{-j\kappa|z-z'|} \\ &- e^{-j\kappa(z+z')} + e^{-j\kappa(2c-(z+z'))} - \varsigma_{z,z'} \cdot e^{-j\kappa(2c-|z-z'|)}) \end{aligned} \quad (\text{C4b})$$

and for the rectangular waveguide (RG1)

$$\mathcal{V}_{\text{RG1},i}(z, z') = -\frac{Z_i}{2} e^{-j\kappa|z-z'|} \quad (\text{C5a})$$

$$\mathcal{I}_{\text{RG1},i}(z, z') = -\frac{1}{2} \varsigma_{z,z'} \cdot e^{-j\kappa|z-z'|} \quad (\text{C5b})$$

where  $\kappa$  and  $Z_i$  are defined as in (A9),(A10) respectively, and  $\varsigma_{z,z'} = \text{sign}(z - z')$ . As it is customary at this point we define the unitless coefficients,

$$\bar{\mathcal{V}}_{\text{CV},i}(z, z') \triangleq 2Y_i \mathcal{V}_{\text{CV},i}(z, z')$$

$$\bar{\mathcal{I}}_{\text{CV},i}(z, z') \triangleq 2\mathcal{I}_{\text{CV},i}(z, z')$$

$$\bar{\mathcal{V}}_{\text{RG1},i}(z, z') \triangleq 2Y_i \mathcal{V}_{\text{RG1},i}(z, z')$$

$$\bar{\mathcal{I}}_{\text{RG1},i}(z, z') \triangleq 2\mathcal{I}_{\text{RG1},i}(z, z')$$

where  $Y_i = 1/Z_i$  denotes the modal admittance. Then, the subtracted fields in the cavity and the rectangular waveguide for  $z$ -oriented magnetic current are given by,

$$E_{xz}^{(1)}(\mathbf{r}, \mathbf{r}') = \frac{j}{ab} \sum_i \frac{\epsilon_n \epsilon_m}{2} (\bar{\mathcal{V}}_{\text{CV},i}(z, z') - \bar{\mathcal{V}}_{\text{RG1},i}(z, z')) \frac{k_y}{\kappa} Co_x(x') Co_y(x') Co_x(x) Si_y(y) \quad (\text{C6a})$$

$$E_{yz}^{(1)}(\mathbf{r}, \mathbf{r}') = \frac{-j}{ab} \sum_i \frac{\epsilon_n \epsilon_m}{2} (\bar{\mathcal{V}}_{\text{CV},i}(z, z') - \bar{\mathcal{V}}_{\text{RG1},i}(z, z')) \frac{k_x}{\kappa} Co_x(x') Co_y(y') Si_x(x) Co_y(y) \quad (\text{C6b})$$

$$E_{zz}^{(1)}(\mathbf{r}, \mathbf{r}') = 0 \quad (\text{C6c})$$

$$H_{xz}^{(1)}(\mathbf{r}, \mathbf{r}') = \frac{j}{\omega \mu ab} \sum_i \frac{\epsilon_n \epsilon_m}{2} (\bar{\mathcal{I}}_{\text{CV},i}(z, z') - \bar{\mathcal{I}}_{\text{RG1},i}(z, z')) k_x Co_x(x') Co_y(y') Si_x(x) Co_y(y) \quad (\text{C6d})$$

$$H_{yz}^{(1)}(\mathbf{r}, \mathbf{r}') = \frac{j}{\omega \mu ab} \sum_i \frac{\epsilon_n \epsilon_m}{2} (\bar{\mathcal{I}}_{\text{CV},i}(z, z') - \bar{\mathcal{I}}_{\text{RG1},i}(z, z')) k_y Co_x(x') Co_y(y') Co_x(x) Si_y(y) \quad (\text{C6e})$$

$$H_{zz}^{(1)}(\mathbf{r}, \mathbf{r}') = \frac{1}{(\omega \mu) ab} \sum_i \frac{\epsilon_n \epsilon_m}{2} (\bar{\mathcal{V}}_{\text{CV},i}(z, z') - \bar{\mathcal{V}}_{\text{RG1},i}(z, z')) \frac{(k_{t,i})^2}{\kappa} Co_x(x') Co_y(y') Co_x(x) Co_y(y) \quad (\text{C6f})$$

b. *2nd form of infinite Rectangular Waveguide (RGW)'s Green's Function and the 1st form of the (infinite) Parallel plate*

Similarly to Sec. ( III A.2), the transverse eigenvectors for E-mode and H-mode problems are obtained from the

scalar potentials expressed in Eqs. (19a),(19b). For the longitudinal problem of the 1D TL along the  $y$ -axis, the sketch (Fig. 3 (b),(d)) is also identical up to the sources: namely, in the RG waveguide (RG2) case the

TL is shorted at its terminations, while in the parallel plate case the TLs are infinite. The modal current source is null in the E- and H-mode cases, whereas the modal voltage source reads for the E-mode

$$v_i(y; \mathbf{r}') = \frac{1}{\sqrt{\pi a}} \frac{\frac{m\pi}{a}}{k'_{t,i}} e^{j\xi z'} \cos\left(\frac{m\pi x'}{a}\right) \delta(y - y') \quad (\text{C7a})$$

and for the H-mode

$$v_i(y; \mathbf{r}') = -\sqrt{\frac{\epsilon_n}{2\pi a}} \frac{j\xi}{k'_{t,i}} e^{j\xi z'} \cos\left(\frac{m\pi x'}{a}\right) \delta(y - y') \quad (\text{C7b})$$

where  $0 \leq m \leq \infty$ , and  $\epsilon_m = 2 - \delta[m]$  as before. In both cases,  $-\infty \leq \xi \leq \infty$ .  $i$  denote a couple  $(\xi, m)$  and  $k_{t,i}^2 = \xi^2 + (m\pi/a)^2$ . The solutions to the TL problem are presented as follows, for the TL model of the rectangular waveguide (RG2)

$$\begin{aligned} \mathcal{V}_{\text{RG2},i}(y, y') &= \frac{1}{2(e^{-2j\kappa b} - 1)} (\zeta_{y,y'} \cdot e^{-j\kappa|y-y'|} \\ &+ e^{-j\kappa(y+y')} - e^{-j\kappa(2b-(y+y'))} - \zeta_{y,y'} \cdot e^{-j\kappa(2b-|y-y'|)}) \end{aligned} \quad (\text{C8a})$$

$$\begin{aligned} \mathcal{I}_{\text{RG2},i}(y, y') &= \frac{1}{2Z_i(e^{-2j\kappa b} - 1)} (e^{-j\kappa|y-y'|} \\ &+ e^{-j\kappa(y+y')} + e^{-j\kappa(2b-(y+y'))} + e^{-j\kappa(2b-|y-y'|)}) \end{aligned} \quad (\text{C8b})$$

and for the parallel plates waveguide (PP1):

$$\mathcal{V}_{\text{PP1},i}(y, y') = \frac{-1}{2} \zeta_{y,y'} \cdot e^{-j\kappa|y-y'|} \quad (\text{C9a})$$

$$\mathcal{I}_{\text{PP1},i}(y, y') = \frac{-Y_i}{2} e^{-j\kappa|y-y'|} \quad (\text{C9b})$$

The unitless amplitudes are extracted as:

$$\begin{aligned} \bar{\mathcal{V}}_{\text{RG2},i}(y, y') &\triangleq 2 \mathcal{V}_{\text{RG2},i}(y, y') \\ \bar{\mathcal{I}}_{\text{RG2},i}(y, y') &\triangleq 2Z_i \mathcal{I}_{\text{RG2},i}(y, y') \\ \bar{\mathcal{V}}_{\text{PP1},i}(y, y') &\triangleq 2 \mathcal{V}_{\text{PP1},i}(y, y') \\ \bar{\mathcal{I}}_{\text{PP1},i}(y, y') &\triangleq 2 \mathcal{I}_{\text{PP1},i}(y, y') \end{aligned}$$

In sum, the subtraction of the parallel plates from the rectangular waveguide fields for a  $z$ -oriented magnetic magnetic current element can be expressed as follows,

$$E_{xz}^{(2)}(\mathbf{r}, \mathbf{r}') = \frac{-1}{2\pi a} \sum_m \frac{\epsilon_m}{2} Co_x(x') Co_x(x) \int_{\xi} d\xi (\bar{\mathcal{V}}_{\text{RG2},i}(y, y') - \bar{\mathcal{V}}_{\text{PP1},i}(y, y')) e^{-j\xi(z-z')} \quad (\text{C10a})$$

$$E_{yz}^{(2)}(\mathbf{r}, \mathbf{r}') = \frac{-j}{2\pi a} \sum_{m \neq 0} Co_x(x') Si_x(x) \int_{\xi} d\xi \frac{k_x}{\kappa} (\bar{\mathcal{I}}_{\text{RG2},i}(y, y') - \bar{\mathcal{I}}_{\text{PP1},i}(y, y')) e^{-j\xi(z-z')} \quad (\text{C10b})$$

$$E_{zz}^{(2)}(\mathbf{r}, \mathbf{r}') = 0 \quad (\text{C10c})$$

$$H_{xz}^{(2)}(\mathbf{r}, \mathbf{r}') = \frac{j}{2\pi a \omega \mu} \sum_{m \neq 0} Co_x(x') Si_x(x) \int_{\xi} d\xi \frac{\xi k_x}{\kappa} (\bar{\mathcal{I}}_{\text{RG2},i}(y, y') - \bar{\mathcal{I}}_{\text{PP1},i}(y, y')) e^{-j\xi(z-z')} \quad (\text{C10d})$$

$$H_{yz}^{(2)}(\mathbf{r}, \mathbf{r}') = \frac{-1}{2\pi a \omega \mu} \sum_m \frac{\epsilon_m}{2} Co_x(x') Co_x(x) \int_{\xi} d\xi \xi (\bar{\mathcal{V}}_{\text{RG2},i}(y, y') - \bar{\mathcal{V}}_{\text{PP1},i}(y, y')) e^{-j\xi(z-z')} \quad (\text{C10e})$$

$$H_{zz}^{(2)}(\mathbf{r}, \mathbf{r}') = \frac{1}{2\pi a \omega \mu} \sum_m \frac{\epsilon_m}{2} Co_x(x') Co_x(x) \int_{\xi} d\xi \frac{\kappa^2 + k_x^2}{\kappa} (\bar{\mathcal{I}}_{\text{RG2},i}(y, y') - \bar{\mathcal{I}}_{\text{PP1},i}(y, y')) e^{-j\xi(z-z')} \quad (\text{C10f})$$

### c. 2nd form of the Parallel Plate's Green's Function and Our Alternative Representation of Free Space Green's Function

The outline of the derivation is identical to the one in Sec. III A.3. The scalar potentials of the boundary problem of the E-mode and the H-mode are given as Eq. (24), from which for the expression of the transverse eigenvectors for the E- and H-mode is then extracted. The modal current source is null in the E- and H-mode cases,

whereas the modal voltage source reads for the E-mode

$$v_i(x; \mathbf{r}') = -\frac{1}{2\pi} \frac{j\eta}{k'_{t,i}} e^{j\eta y'} e^{j\xi z'} \delta(x - x') \quad (\text{C11a})$$

and for the H-Mode

$$v_i(x; \mathbf{r}') = -\frac{1}{2\pi} \frac{j\xi}{k'_{t,i}} e^{j\eta y'} e^{j\xi z'} \delta(x - x') \quad (\text{C11b})$$

The description in Fig. 4(b),(d) of the type of terminations still holds. Further, the TL problem can readily

be solved for the parallel plates (PP2)

$$\begin{aligned} \mathcal{V}_{\text{PP2},i}(x, x') &= \frac{1}{2(e^{-2j\kappa a} - 1)} (\zeta_{x,x'} \cdot e^{-j\kappa|x-x'|} \\ &+ e^{-j\kappa(x+x')} - e^{-j\kappa(2a-(x+x'))} - \zeta_{x,x'} \cdot e^{-j\kappa(2a-|x-x'|)}) \end{aligned} \quad (\text{C12a})$$

$$\begin{aligned} \mathcal{I}_{\text{PP2},i}(x, x') &= \frac{1}{2Z_i(e^{-2j\kappa b} - 1)} (e^{-j\kappa|x-x'|} \\ &+ e^{-j\kappa(x+x')} + e^{-j\kappa(2b-(x+x'))} + e^{-j\kappa(2b-|x-x'|)}) \end{aligned} \quad (\text{C12b})$$

and for the free space:

$$\mathcal{V}_{\text{FS},i}(x, x') = \frac{-1}{2} \zeta_{x,x'} \cdot e^{-j\kappa|x-x'|} \quad (\text{C13a})$$

$$\mathcal{I}_{\text{FS},i}(x, x') = \frac{-1}{2Z_i} e^{-j\kappa|x-x'|} \quad (\text{C13b})$$

The corresponding unitless amplitudes are extracted as:

$$\begin{aligned} \bar{\mathcal{V}}_{\text{PP2},i}(x, x') &\triangleq 2 \mathcal{V}_{\text{PP2},i}(x, x') \\ \bar{\mathcal{I}}_{\text{PP2},i}(x, x') &\triangleq 2Z_i \mathcal{I}_{\text{PP2},i}(x, x') \\ \bar{\mathcal{V}}_{\text{FS},i}(x, x') &\triangleq 2 \mathcal{V}_{\text{FS},i}(x, x') \\ \bar{\mathcal{I}}_{\text{FS},i}(x, x') &\triangleq 2 \mathcal{I}_{\text{FS},i}(x, x') \end{aligned}$$

Finally, the dyadic Green's functions for a z-oriented magnetic current inside the parallel plate and in free space can be expressed as follows,

$$E_{xz}^{(3)}(\mathbf{r}, \mathbf{r}') = \frac{j}{4\pi} \sin(\bar{\phi}) \int_{\infty} dq \frac{q^2}{\kappa} \mathcal{J}_1(q\bar{\rho}) (\bar{\mathcal{I}}_{\text{PP2},i}(x, x') - \bar{\mathcal{I}}_{\text{FS},i}(x, x')) \quad (\text{C14a})$$

$$E_{yz}^{(3)}(\mathbf{r}, \mathbf{r}') = \frac{1}{4\pi} \int_{\infty} dq q \mathcal{J}_0(q\bar{\rho}) (\bar{\mathcal{V}}_{\text{PP2},i}(x, x') - \bar{\mathcal{V}}_{\text{FS},i}(x, x')) \quad (\text{C14b})$$

$$E_{zz}^{(3)}(\mathbf{r}, \mathbf{r}') = 0 \quad (\text{C14c})$$

$$H_{xz}^{(3)}(\mathbf{r}, \mathbf{r}') = \frac{j}{4\pi} \frac{\cos(\bar{\phi})}{\omega\mu} \int_{\infty} dq q^2 \mathcal{J}_1(q\bar{\rho}) (\bar{\mathcal{V}}_{\text{PP2},i}(x, x') - \bar{\mathcal{V}}_{\text{FS},i}(x, x')) \quad (\text{C14d})$$

$$H_{yz}^{(3)}(\mathbf{r}, \mathbf{r}') = \frac{1}{8\pi} \frac{\sin(2\bar{\phi})}{\omega\mu} \int_{\infty} dq \frac{q^3}{\kappa} \mathcal{J}_2(q\bar{\rho}) (\bar{\mathcal{I}}_{\text{PP2},i}(x, x') - \bar{\mathcal{I}}_{\text{FS},i}(x, x')) \quad (\text{C14e})$$

$$H_{zz}^{(3)}(\mathbf{r}, \mathbf{r}') = \frac{1}{8\pi\omega\mu} \int_{\infty} dq [\frac{q^3}{\kappa} \mathcal{J}_2(q\bar{\rho}) \cos(2\bar{\phi}) + \frac{q}{\kappa} (2k^2 - q^2) \mathcal{J}_0(q\bar{\rho})] (\bar{\mathcal{I}}_{\text{PP2},i}(x, x') - \bar{\mathcal{I}}_{\text{FS},i}(x, x')) \quad (\text{C14f})$$

Lastly, the complete local field can be expressed by adding the three subtraction terms. For instance, the full expression for the dyadic Green's function entries for the  $x$ -component of electric field and magnetic field due

to a magnetic current element in  $\hat{z}$  are given by,

$$\mathbf{G}_{\mathbf{x}\mathbf{z}}^{hh}(\mathbf{r}, \mathbf{r}') = \hat{\mathbf{x}}\hat{\mathbf{z}}(H_{xz}^{(1)} + H_{xz}^{(2)} + H_{xz}^{(3)}) \quad (\text{C15a})$$

$$\mathbf{G}_{\mathbf{x}\mathbf{z}}^{eh}(\mathbf{r}, \mathbf{r}') = \hat{\mathbf{x}}\hat{\mathbf{z}}(E_{xz}^{(1)} + E_{xz}^{(2)} + E_{xz}^{(3)}) \quad (\text{C15b})$$

where  $\hat{\mathbf{x}}\hat{\mathbf{z}}$  represents a dyadic product.

---

[1] A. O. Govorov, *The Journal of Physical Chemistry C* **115**, 7914 (2011).

[2] H. Zhang and A. O. Govorov, *Physical Review B* **87**, 075410 (2013).

[3] Y.-C. Liu, B.-B. Li, and Y.-F. Xiao, *Nanophotonics* **6**, 789 (2017).

[4] C.-R. Mann, T. J. Sturges, G. Weick, W. L. Barnes, and E. Mariani, *Nature Communications* **9**, 2194 (2018).

[5] A. M. Armani, R. P. Kulkarni, S. E. Fraser, R. C. Flagan, and K. J. Vahala, *Science* **317**, 783 (2007).

[6] S. Huang and G. S. Agarwal, *Physical Review A* **83**, 043826 (2011).

[7] C.-R. Mann and E. Mariani, *Physical Review Research* **4**, 013078 (2022).

[8] E. M. Purcell, in *Proceedings of the American Physical Society* (1946) presented at the American Physical Society Meeting, 1946.

[9] D. Kleppner, *Physical Review Letters* **47**, 233 (1981).

[10] R. G. Hulet, E. S. Hilfer, and D. Kleppner, *Physical Review Letters* **55**, 2137 (1985).

[11] E. Yablonovitch, *Physical Review Letters* **58**, 2059 (1987).

[12] G. Gabrielse and H. Dehmelt, *Physical Review Letters* **55**, 67 (1985).

[13] D. Englund, D. Fattal, E. Waks, G. Solomon, B. Zhang, T. Nakaoka, Y. Arakawa, Y. Yamamoto, and J. Vuck-

ovic, Physical Review Letters **95**, 013904 (2005).

[14] Y. Hadad and N. Engheta, Proceedings of the National Academy of Sciences **117**, 5576 (2020).

[15] G. Chiriacó, arXiv preprint arXiv:2310.15184 (2023).

[16] J. M. Wylie and J. E. Sipe, Phys. Rev. A **30**, 1185 (1984).

[17] J. M. Wylie and J. E. Sipe, Phys. Rev. A **32**, 2030 (1985).

[18] S. Mukamel, A. Li, and M. Galperin, The Journal of Chemical Physics **158**, 154106 (2023).

[19] J. George, T. Chervy, A. Shalabney, E. Devaux, H. Hiura, C. Genet, and T. W. Ebbesen, Physical Review Letters **117**, 153601 (2016).

[20] T. Schwartz, J. A. Hutchison, C. Genet, and T. W. Ebbesen, Physical Review Letters **106**, 196405 (2011).

[21] J. Flick, N. Rivera, and P. Narang, Nanophotonics **7**, 1479 (2018).

[22] R. F. Ribeiro, L. A. Martínez-Martínez, M. Du, J. Campos-Gonzalez-Angulo, and J. Yuen-Zhou, Chemical Science **9**, 6325 (2018).

[23] S. Kéna-Cohen and J. Yuen-Zhou, ACS Central Science **5**, 386 (2019).

[24] C. L. Degen, F. Reinhard, and P. Cappellaro, Reviews of Modern Physics **89**, 035002 (2017).

[25] X. Zhang, C.-L. Zou, L. Jiang, and H. X. Tang, Physical Review Letters **113**, 156401 (2014).

[26] A. Reiserer and G. Rempe, Reviews of Modern Physics **87**, 1379 (2015).

[27] T. D. Ladd, F. Jelezko, R. Laflamme, Y. Nakamura, C. Monroe, and J. L. O'Brien, Nature **464**, 45 (2010).

[28] C. C. Gerry and P. L. Knight, *Introductory Quantum Optics*, 2nd ed. (Cambridge University Press, Cambridge, United Kingdom, 2024).

[29] J. Larson and T. Mavrogordatos, *The Jaynes-Cummings Model and Its Descendants* (Institute of Physics Publishing, 2023).

[30] C. Sánchez Muñoz, F. Nori, and S. De Liberato, Nature Communications **9**, 1924 (2018).

[31] A. Peterson, S. Ray, and R. Mittra, *Computational Methods for Electromagnetics* (Universities Press, 2001).

[32] L. Novotny and B. Hecht, *Principles of Nano-Optics*, second edition ed. (Cambridge University Press, Cambridge, New York, Melbourne, Madrid, Cape Town, Singapore, São Paulo, Delhi, Mexico City, 2012).

[33] S. Steshenko, F. Capolino, P. Alitalo, and S. Tretyakov, Physical Review E **84**, 016607 (2011).

[34] M. Born, E. Wolf, and A. Bhatia, *Principles of Optics*: *Electromagnetic Theory of Propagation, Interference and Diffraction of Light* (Cambridge University Press, 1999).

[35] J. D. Jackson, *Classical Electrodynamics*, 3rd ed. (John Wiley & Sons, 1999) chap.9, Sect.6.

[36] R. E. Collin, *Field Theory of Guided Waves*, 2nd ed. (McGraw-Hill, IEEE, 1991).

[37] A. Yaghjian, Proceedings of the IEEE **68**, 248 (1980).

[38] K. E. Jordan, G. R. Richter, and P. Sheng, Journal of Computational Physics **63**, 222 (1986).

[39] F. Capolino, D. Wilton, and W. Johnson, Journal of Computational Physics **223**, 250 (2007).

[40] F. T. Celepcikay, D. R. Wilton, D. R. Jackson, and F. Capolino, Radio Science **43**, RS6S01 (2008).

[41] D. Beutel, I. Fernandez-Corbaton, and C. Rockstuhl, Physical Review A **107**, 013508 (2023).

[42] M.-J. Park, J. Park, and S. Nam, IEEE Microwave and Guided Wave Letters **8**, 124 (1998).

[43] S. Campione, S. Steshenko, M. Albani, and F. Capolino, Optics Express **19**, 26027 (2011).

[44] S. Campione and F. Capolino, Radio Science **47**, RS0N06 (2012).

[45] Y. Mazor and B. Z. Steinberg, Physical Review Letters **112**, 153901 (2014).

[46] L. B. Felsen and N. Marcuvitz, *Radiation and Scattering of Waves* (Wiley-IEEE Press, 2001).

[47] A. Ishimaru, *Electromagnetic Wave Propagation, Radiation, and Scattering* (Prentice Hall, Englewood Cliffs, NJ, 1991).

[48] K.-E. Sadzi and Y. Hadad, “Loss vs magnetization threshold phenomenon for lorentz nonreciprocity induced by a gyrotropic particle inside a cavity,” (2024), preprint.

[49] Y. Hadad and B. Z. Steinberg, Physical Review Letters (2010).

[50] A. Canaguier-Durand and C. Genet, Physical Review A **92**, 043823 (2015).

[51] J. Mun, M. Kim, Y. Yang, T. Badloe, J. Ni, Y. Chen, C. W. Qiu, and J. Rho, Light: Science & Applications **9**, 139 (2020).

[52] D. R. Smith and N. Kroll, Phys. Rev. Lett. **85**, 2933 (2000).

[53] T. J. Cui and J. A. Kong, Phys. Rev. B **70**, 205106 (2004).

[54] A. D. Boardman and K. Marinov, Physical Review B **73**, 165110 (2006).